SEMILEPTONIC $B \to D$ DECAY AT NONZERO RECOIL WITH 2+1 FLAVOR OF IMPROVED STAGGERED QUARKS

by

Siwei Qiu

A dissertation submitted to the faculty of
The University of Utah
in partial fulfillment of the requirements for the degree of

Doctor of Philosophy

in

Physics

Department of Physics and Astronomy

The University of Utah

December 2013

The University of Utah Graduate School

STATEMENT OF DISSERTATION APPROVAL

The dissertation of Siwei Qiu
has been approved by the following supervisory committee members:

Carleton DeTar , Chair	August 23, 2013
	Date Approved
Oleg Starykh , Member	August 23, 2013
	Date Approved
Yong-Shi Wu , Member	August 23, 2013
	Date Approved
Stephen Lebohec , Member	August 23, 2013
	Date Approved
Aaron L Fogelson , Member	August 23, 2013
	Date Approved

and by Carleton DeTar, Chair/Dean of the Department/College/School of Physics and Astronomy and by David B. Kieda, Dean of The Graduate School.

ABSTRACT

The purpose of this thesis is to carry out a precise test of the standard model of particle physics, *i.e.,* the model that describes the strong and electroweak interactions between quarks, leptons, and gauge bosons. Such a precision test may well lead to the discovery of new physics beyond the standard model. More specifically, this thesis gives a precise determination of $|V_{cb}|$, one of the parameters of the standard model which controls the semileptonic decay process $B \to Dl\nu$. This parameter is one of several that make up the CKM matrix. If the standard model is correct, that matrix must be unitary. A deviation from unitarity would be a sign of new physics. Although this is mainly an electroweak process, it occurs in the environment of the strong interactions. The strong interaction effects are encoded in the form factor $\mathcal{G}$, for the vector current transition from the B meson to the D meson. In this thesis, we calculate the form factor. Experimental measurements provide the product $\mathcal{G}|V_{cb}|$. So theory and experiment together give $|V_{cb}|$. We calculate the form factor in a numerical simulation, using lattice quantum chromodynamics. Ours is the first numerical calculation of the full form factor (nonzero recoil) that takes into account all the effects of the strong interactions (including sea quarks) and carries out an extrapolation to physical quark masses in the limit of zero lattice spacing. We give the theoretical backgound of the calculation, describe our data analysis, give a detailed analysis of all sources of error, and fit our result and the experimental data from the Babar collaboration to get our final result, namely, $|V_{cb}| = 0.0402(20)$.

To my wife and my parents.

CONTENTS

LIST OF FIGURES

LIST OF TABLES

ACKNOWLEDGEMENTS

Computations generating the gauge field ensembles and the two-point and three-point correlators were carried out with resources provided by the USQCD Collaboration, the National Energy Research Scientific Computing Center, and the Argonne Leadership Computing Facility, which is funded by the Office of Science of the U.S. Department of Energy; and with resources provided by the National Institute for Computational Science and the Texas Advanced Computing Center, which are funded through the National Science Foundation's Teragrid/XSEDE Program. We thank our colleagues in the Fermilab Lattice and MILC collaborations for providing these data for use in this thesis. This work is supported in part by the U.S. National Science Foundation under grants PHY0757333 and PHYS1067881 and PHY0903571. Analysis computation for this thesis were carried out with computer resources of the Department of Physics and Astronomy, University of Utah.

CHAPTER 1

INTRODUCTION

The standard model of particle physics is a field theoretical description of the strong and electroweak interactions. It has been enormously successful in explaining experimental results thus far — *i.e.*, up to energy scales of 1 TeV. However, empirical evidence suggests that the standard model is incomplete and there is a more fundamental theory to be discovered. This is called "physics beyond the standard model." We list some reasons that we expect that there is physics beyond the standard model. The existence of nonbaryonic dark matter calls for physics beyond the standard model, since none of the particles in the standard model are suitable candidates for dark matter. Dark energy may be related to gravity. However, gravity is not unified with the standard model, making the theory seem incomplete. A successful unification awaits physics beyond the standard model. The universe is dominated by matter with little antimatter; such an asymmetry also suggests that there should be physics beyond the standard model, since the standard model predicts that there is no net baryon number in the universe.

There are some philosophical and esthetic arguments that call for physics beyond the standard model. In the standard model, the Higgs bosons is an elementary scalar particle. In quantum field theory, such particles have problems. The Higgs particle has a quadratic divergent self energy which could be mitigated by introducing new fundamental particles. For example, one of the ways to deal with such a problem is to introduce supersymmetric particles. This then leads to new physics beyond the standard model. Then there are unexplained parameters and features. Why is the QCD theta-term so small or even zero? The standard model does not explain it.

Precision tests can give clues about new physics at high energy scales. For example, the $K - \overline{K}$ system revealed a small CP violation, the violation of the symmetry of charge conjugation and parity [4]. CP violation results from physics at a high energy scale, but we can already test it with relatively low energy physics. This achievement leads us to believe that new physics can be seen if we have more precise experimental measurements combined

with precise theoretical determinations of important physical quantities, such as CKM matrix elements. This thesis is devoted to a precise determination of one of the CKM matrix elements, $|V_{cb}|$, which is a parameter of the standard model that controls the semileptonic decay $B \to Dl\nu$. Fundamentally, this decay involves the transition from a b quark to a c quark. We use numerical simulation to calculate the strong interaction environment of this semileptonic decay. This allows us to extract the value of $|V_{cb}|$ from experimental measurements of the decay. The strong interaction environment is characterized by a *form factor*. The numerical simulation uses a lattice version of quantum chromodynamics, or *Lattice QCD*. It is a nonperturbative *ab initio* method, capable of giving an accurate prediction of QCD. Experiment measures the product of $|V_{cb}|$ and the form factor. One can divide the experimental results by the theoretical results for the form factor to extract $|V_{cb}|$. $|V_{cb}|$ is one of the important parameters in particle physics, which is needed in the determination of other parameters, such as ϵ_K in kaon physics [5]. So the uncertainty in $|V_{cb}|$ contributes to the uncertainty in ϵ_K. One can obtain a better determination of ϵ_K through lattice calculation of the matrix element of $K \to \pi\pi$. We will talk about this in more detail in Chapter 3.

There are a variety of ways to get a decay form factor experimentally or theoretically and thereby determine $|V_{cb}|$. One method is through the "inclusive" process, *i.e.*, the decay $B \to X_c l\nu$, where X_c denotes any charmed final state, such as $D\pi$ or $D\pi\pi$, etc. It is popular to use the operator product expansion and heavy quark symmetry to estimate the inclusive form factor, which, combined with the experimental measurement, gives the "inclusive determination" of $|V_{cb}|$.

Another method, the exclusive method, uses specific decay channels, such as $B \to Dl\nu$ or $B \to D^* l\nu$. For the $B \to D^* l\nu$ exclusive calculation, some theorists make use of the operator product expansion to estimate the exclusive form factor, but lattice QCD is now the preferred method. For the lattice calculation of exclusive $B \to Dl\nu$, Hashimoto *et al.* [6] have done a calculation to determine $|V_{cb}|$ based on the form factor at zero recoil, that is for the case where the B and D mesons have the same velocity. In this paper, we will extend this method to nonzero recoil data. Ours is the first nonzero recoil calculation with full treatment of QCD. A calculation at nonzero recoil is preferable because, for kinematic reasons, there are very few decays at zero recoil. So if we have a good determination of form factor at nonzero recoil, we may hope to get a small error for $|V_{cb}|$ when we combine results from experiment and lattice.

Of course, both inclusive and exclusive determinations of $|V_{cb}|$ should agree. At present,

the inclusive and exclusive determinations of $|V_{cb}|$ disagree by two standard deviations. The inclusive determination gives $= (42.42 \pm 0.86) \times 10^3$ [7], whereas exclusive determination gives $(0.0390(5)_{\text{theory}}(5)_{\text{experiment}}(2)_{EW}$ [8]. The purpose of this work is to reduce the error in the exclusive determination.

This thesis is organized as follows: In Chapter 2, we give some background about the standard model of particle physics. In Chapter 3, we discuss the unitarity constraint on the CKM matrix, the determination of the unitarity triangle, disagreement between different methods, and measurement of the decay rate of $B \to Dl\nu$. In Chapter 4, we introduce lattice gauge theory, the numerical method we use, discuss the lattice data we generated and the computation of the lattice form factor. To emphasize, the lattice data here are blinded to avoid bias when we determine the form factor. And when we finally get the new value of $|V_{cb}|$, we will unblind it. In Chapter 5, we present our analysis of the simulation results and report the value of $|V_{cb}|$ and form factors.

CHAPTER 2

STANDARD MODEL

In this chapter, we give a brief introduction to the standard model of particle physics. The standard model tells us about the most elementary particles known to date and interactions between them. After this introduction, we can discuss semileptonic decay, the main topic of my thesis.

2.1 Standard model

The standard model of particle physics [9] is one of the remarkable achievements of the 20th century. It describes strong and electroweak interactions. The various elementary particles are shown in Figure 2.1. There are quarks, leptons, the gauge bosons, and the Higgs boson. In this figure, the first three columns represent three "generations" of quarks. The upper row u, c, and t have charge $2/3e$, and the lower row d, s, and b have charge $-1/3e$. The labels up, charm, top, down, strange, bottom, or c, t, d, s, b, respectively, are called "flavors." The first two generations of quarks have small mass, few MeV/c^2, or 1 GeV/c^2; however, the third generation of quark is heavier, as high as 173 GeV/c^2. Also, there are three generations of leptons. The leptons, e, μ, and τ, have charge -1, and the corresponding three neutrinos have no charge. Then there are gauge bosons, namely the photon, gluon, Z boson, and W bosons. Finally, there is the Higgs boson, which was discovered at the LHC experiment recently. In the $B \to Dl\nu$ process we are considering, the "l" is one of the charged leptons e^-, μ^- , τ^- and the neutrino ν_e, ν_μ, ν_τ matches the electron. We focus on just $l = e^-$ and μ^- in this thesis.

2.1.1 Strong interaction

Now, we introduce the different interactions of the standard model one by one. First we introduce the strong interaction or quantum chromodynamics (QCD), the theory that we simulate numerically [11][12]. The interaction between the quarks is through the strong interaction. QCD is a gauge theory with gauge group $SU(3)$. The gauge boson is the gluon.

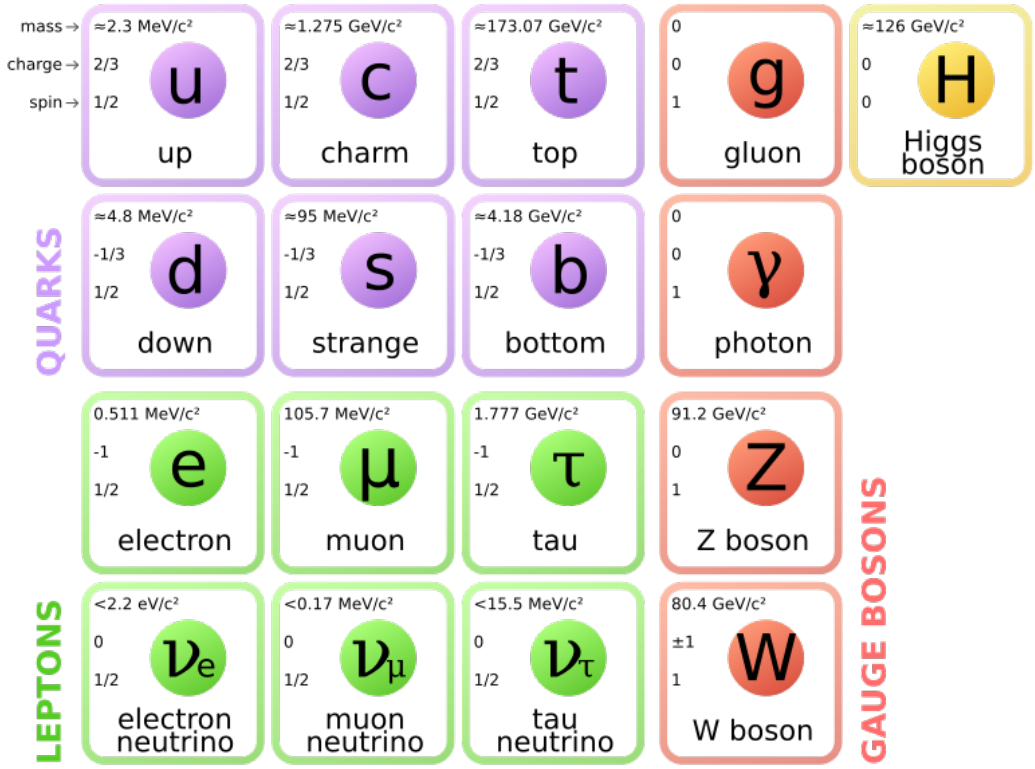

Figure 2.1. Particles in the standard model [10].

All quarks interact by exchanging color charge. The gluon also carries color charge. In the framework of field theory, the interactions are described by terms in the Lagrangian:

$$\begin{aligned} \mathcal{L} &= \sum_{i=1}^{N_f} [\overline{\Psi}_{i,d}(x)(\not{D} + m_i)_{de}\Psi_{i,e}(x)] - \frac{1}{4}F_{\mu\nu,a}F^{\mu\nu,a} \\ F_{\mu\nu,a} &= \partial_\mu A_{\nu,a} - \partial_\nu A_{\mu,a} - g f_{abc} A_{\mu,b} A_{\nu,c} \\ D_\mu \psi &= (\partial_\mu + igA_{\mu,a}\frac{\lambda_a}{2})\psi \ . \end{aligned} \tag{2.1}$$

The sum is over N_f flavors. $\Psi_{i,d}$ is the Dirac spinor for a quark with flavor i and color d, while $F_{\mu\nu,a}$ is the color field tensor, which represents the gluon in QCD theory. Here, a is an index for eight colors, corresponding to the eight generators of the $SU(3)$ group. The coupling parameter is g. f_{abc} and $\lambda_a/2$ are the structure constants and generators of $SU(3)$ group, respectively. $\not{D}_{de}$ is $(\gamma_\mu D^\mu)_{de}$. D is the covariant derivative. Here, m_i is mass of the quark for flavor i.

The D^0 and D^{0*} mesons have a charm (c) quark and anti up ($\overline{u}$) quark. The D^+ and $D^{*,+}$ mesons have a charm (c) quark and anti down ($\overline{d}$) quark. The D^0 and D^+ have angular momentum 0 and negative parity, and the D^{*0} and D^{*+}, angular momentum 1 and negative parity. The D^{*0} contains the same quarks as D^0. When we change charm quark

in the D meson to bottom quark, we have $\overline{B}^0$, B^+, $\overline{B^{0*}}$, and B^{*+}. So the B and D meson are both pesudoscalar mesons, while the B^* and D^* are vector mesons.

2.1.2 Electroweak interaction

The electroweak interaction [13] is traditionally separated into the electromagnetic interaction and the weak interaction. The electromagnetic interaction involves interactions between photons and charged particles. It includes quantum electrodynamics (QED) [14], the theory of interacting electrons and photons. In the standard model, this interaction is unified with the weak interactions. The difference is (1) the weak interaction exchanges W or Z bosons instead of a photon, (2) the weak interaction includes the leptons, and (3) the weak interaction can change the quark flavor. The electromatnetic (EM) interaction is relevant to my work slightly, since the exchange of photon can give a small correction to the decay of the $B^0 \to D^- l^+ \nu$. The unified electroweak theory was introduced by Glashow, Weinberg, and Salam in 1967. They were awarded the Nobel Prize in physics in 1979. We describe the theory in more detail in the following paragraphs, since the $B \to Dl\nu$ process is a weak process.

The semileptonic decay is caused by the electroweak interaction, as shown in Figure 2.2. In this figure, we see the hadronic part, $b \to c$, together with the spectator light quark $\overline{d}$. These quarks are interacting by strong interaction. We also have the lepton part, containing the electron or muon, together with the neutrino. We will introduce the amplitude of this process in the next chapter.

With group structure of $SU(2)_L \times U(1)$, the electroweak model describes weak isospin and weak hypercharge, respectively. An important charateristic of weak interactions is the violation of parity. In our notation, we use L to denote left-handed, which means at high velocity, spin and momentum have opposite direction. We also say left-handed particles have negative helicity, while right-handed particles have positive helicity. The Lagrangian of the electroweak interaction can be divided into three parts, namely the gauge-field, fermion-field, and Higgs-field parts:

$$\mathcal{L}_{EW} = \mathcal{L}_G + \mathcal{L}_F + \mathcal{L}_H \ . \tag{2.2}$$

The gauge boson fields that couple to the weak isospin and weak hyercharge are $\overrightarrow{W_\mu} = (W_\mu^1, W_\mu^2, W_\mu^3)$ and B_μ, respectively, and we have the following gauge-field Lagrange density:

$$\mathcal{L}_G = -\frac{1}{4}(F_i^{\mu\nu})^2 - \frac{1}{4}B^{\mu\nu}B_{\mu\nu} \ . \tag{2.3}$$

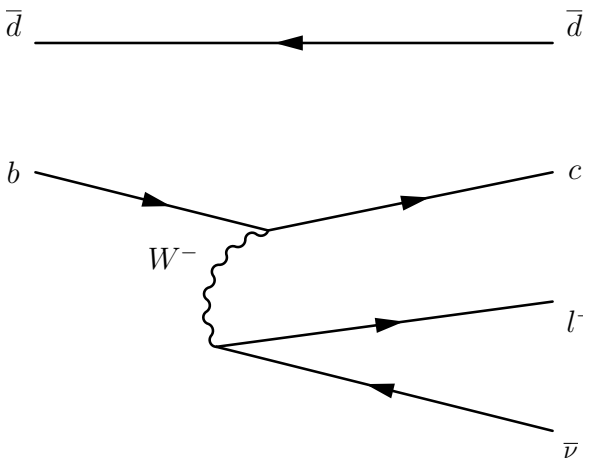

Figure 2.2. Feynman diagram for $B^0 \to D^+ e^- \overline{\nu}_e$. The $b\overline{d}$ is $\overline{B}^0$, and the $c\overline{d}$ is D^+
.

$F^i_{\mu\nu} (i = 1, 2, 3)$ is the $SU(2)$ field strength,

$$F^i_{\mu\nu} = \partial_\mu W^i_\nu - \partial_\nu W^i_\mu - g_2 \epsilon^{ijk} W^j_\mu W^k_\nu \ , \tag{2.4}$$

and $B_{\mu\nu}$ is the $U(1)$ field strength,

$$B_{\mu\nu} = \partial_\mu B_\nu - \partial_\nu B_\mu \ . \tag{2.5}$$

One of the couplings, g_2, appears in Equation (2.4).

For the fermionic sector, we sum over the left-handed weak isodoublets ψ_L. They are the pairs $(u, d)_L$, $(e^+, \overline{\nu_e})$. Also, we sum over the right-handed weak isosinglet, the isotopic singlic state, ψ_R. The Lagrange density is:

$$\mathcal{L}_F = \sum_{\psi_L} \overline{\psi}_L i \not{D} \psi_L + \sum_{\psi_R} \overline{\psi}_R i \not{D} \psi_R \ , \tag{2.6}$$

where the covariant derivative for right-handed chiral fermions is:

$$D_\mu \psi_R = (\partial_\mu + i \frac{g_1}{2} Y_w B_\mu) \psi_R \ , \tag{2.7}$$

and for left-handed fermions, it is:

$$D_\mu \psi_L = \left(I(\partial_\mu + i \frac{g_1}{2} Y_w B_\mu) + i g_2 \frac{\vec{\tau}}{2} \vec{W}_\mu \right) \psi_L \ . \tag{2.8}$$

Both couplings g_1 and g_2 appear. Y_w is the quantum number of weak hypercharge.

The $SU(2)_L \times U(1)$ symmetry is spontaneously broken. This process generates masses for fermion and gauge bosons. After symmetry breaking, it is convenient to introduce two new fields, Z_μ and A_μ, to replace W_μ^3 and B. These represent the massive Z boson (90 GeV/c^2) and photon, respectively. The charged bosons $W_\mu^\pm$ are a linear combination of W_μ^1 and W_μ^2 with masses (80.4 Gev/c^2). The fermions get mass terms, *e.g.,* for the up quark and down quark:

$$-m_d \overline{d}_L d_R - m_u \overline{u}_L u_R + h.c. \; . \tag{2.9}$$

Here, the $u_{L,R}$ and $d_{L,R}$ are mass eigenstates. For a more general mass term, we define the quark mass matrices:

$$\begin{aligned} \mathbf{m}_u &= \begin{pmatrix} m_u & 0 & \\ 0 & m_c & 0 \\ 0 & 0 & m_t \end{pmatrix} \\ \mathbf{m}_d &= \begin{pmatrix} m_d & 0 & \\ 0 & m_s & 0 \\ 0 & 0 & m_b \end{pmatrix} \; . \end{aligned} \tag{2.10}$$

We also define U to be $\{u, t, c\}$, the quarks with charge 2/3; and D to be $\{d, b, s\}$, the quarks with charge $-1/3$. Then we can write Equation (2.9) as follows:

$$-\overline{D}\mathbf{m}_d D - \overline{U}\mathbf{m}_u U + h.c. \; . \tag{2.11}$$

2.2 CKM matrix

With these preliminaries we are ready to discuss semileptonic decays and the CKM matrix. First we identify the terms responsible for the flavor-changing transitions. Then we discuss quark mixing and the CKM matrix.

2.2.1 Flavor changing interaction

In the Lagrangian of the electroweak model, we consider the interaction between the gauge field and the fermion field. From Equation (2.6), we find the following interaction terms:

$$\mathcal{L}_{int} = -\frac{g_2}{\sqrt{8}} \left(W_\mu^+ \mathcal{V}_{ch}^\mu + W_\mu^- \mathcal{V}_{ch}^{\mu\dagger} \right) + ... \tag{2.12}$$

Here, we introduce the charged weak current $\mathcal{V}_{ch}^\mu$. The charged weak current $\mathcal{V}_{ch}^\mu = \mathcal{V}_{ch}^\mu(l) + \mathcal{V}_{ch}^\mu(q)$, *i.e.,* both the lepton part and the quark part, which we now discuss.

A key point is that the states which appear in the original gauge-invariant Lagrangian are generally not the mass eigenstates, but they are unitary linear combinations of them. This is called "mixing":

$$\begin{aligned} U'_{L,\alpha} &= S^u_L U_{L,\alpha} \\ D'_{L,\alpha} &= S^d_L D_{L,\alpha} \ . \end{aligned} \tag{2.13}$$

Here, S^u_L and S^d_L are unitary matrices.

So the quark part of the charged current is:

$$\mathcal{V}^\mu_{ch}(q) = 2\overline{U}'_{L,\alpha}\gamma^\mu D'_{L,\alpha} \ . \tag{2.14}$$

For the lepton part, if we use the following notation to denote the mass eigenstate:

$$\vec{\nu}_L = (\nu_e, \nu_\mu, \nu_\tau)_L \ , \tag{2.15}$$

Then, we use the following notation to denote the gauge eigenstate:

$$\vec{\nu}'_L = (\nu'_e, \nu'_\mu, \nu'_\tau)_L \ . \tag{2.16}$$

Then, we have the lepton part of a charged weak current as follow:

$$\mathcal{V}^\mu_{ch}(l) = 2\vec{\nu}'_{L,\alpha}\gamma^\mu e'_{L,\alpha} \ . \tag{2.17}$$

With this notation, α gives the degree of freedom of lepton generations.

In terms of the mass eigenstates U_L and D_L, the flavor changing current is then:

$$\mathcal{V}^\mu_{ch} = 2\overline{U}_L\gamma^\mu S^{u\dagger}_L S^d_L D_L \ . \tag{2.18}$$

So the transition is described by $V \equiv S^{u\dagger}_L S^d_L$, the CKM matrix, named after Cabibbo, Kobayashi, and Maskawa:

$$V = \begin{pmatrix} \boldsymbol{V_{ud}} & \boldsymbol{V_{us}} & \boldsymbol{V_{ub}} \\ \boldsymbol{V_{cd}} & \boldsymbol{V_{cs}} & \boldsymbol{V_{cb}} \\ \boldsymbol{V_{td}} & \boldsymbol{V_{ts}} & \boldsymbol{V_{tb}} \end{pmatrix} \ . \tag{2.19}$$

If we had only two generations, this is called Cabibbo matrix for the two flavors. Since the two-generation Cabibbo matrix does not explain CP violation, Kobayashi and Maskawa proposed the CKM matrix, the generalization to three flavors. This matrix connects the weak eigenstates (d', s', b') and the corresponding mass eigenstates (d, s, b).

As we show in Figure 2.2, we consider the hadronic part and leptonic part of the four fermion interaction, where we can introduce the Fermi constant G_F. We have the b quark and c quark, which are interacting through the weak interaction vertex, $\mathcal{V}^\mu$.

We can write down the Feynman rule of the the vertex and propagater of the W boson. The vertex bW^-c is as follows:

$$\frac{ig_2}{2\sqrt{2}}V_{cb}\gamma_\mu \ , \tag{2.20}$$

while the vertex $l^-W^-\overline{\nu}$ is as follows:

$$\frac{ig_2}{2\sqrt{2}}\gamma_\mu(1-\gamma_5) \ . \tag{2.21}$$

Based on the fact that momentum transfer q^2 is much smaller than m_W^2, the propagator of the W boson is as follows:

$$-\frac{1}{m_W^2} \ . \tag{2.22}$$

Then, the propagator of the W boson can be absorbed into the Fermi constant, defined as follow:

$$\frac{G_F}{\sqrt{2}} = \frac{g_2^2}{8m_W^2} \ . \tag{2.23}$$

Putting all these pieces together, we can have the following amplitude:

$$\mathcal{A} = \frac{G_F V_{cb}}{\sqrt{2}}\langle D(p')|\mathcal{V}^\mu|\overline{B}(p)\rangle\overline{u}(k_1)\gamma_\mu(1-\gamma_5)v(k_2) \ . \tag{2.24}$$

where $\overline{u}$ is the neutrino spinor, v is the electron or muon spinor.

We will discuss more about $B \to Dl\nu$ process in the next chapter.

2.3 Parameterization of the CKM matrix

The CKM matrix is given in Equation (2.19). We need to consider the number of parameters it represents. It is unitary. Mathematically, an $n \times n$ unitary matrix has n^2 real-valued parameters [15]. Among them, $n(n-1)/2$ are mixing angles. This is because we have $n(n-1)/2$ pairs of different generations. Then, the rest of them, $n^2 - n(n-1)/2 = (n+1)n/2$, are complex phases. To count the complex phases, we need to consider the so-called *quark rephasing* freedom. By quark rephasing, we mean using the freedom of redefining $U_{L,\alpha} \to e^{i\theta_\alpha^u}U_{L,\alpha}$. Here, we use α to denote flavor number. The quarks U and D both have n degree of freedom (n generations), but an overall phase transformation will not make a new degree of freedom, so $2n-1$ of them can be removed by quark rephasing. So there are only $(n-1)(n-2)/2$ phases.

Therefore, in the 2×2 matrix, there is only one parameter and no phases, for example, the θ_c in Cabibbo's formulation. In the 3×3 matrix, there are three parameters, θ_1, θ_2, and θ_3 and one phase δ [16].

Define $s_\alpha \equiv \sin\theta_\alpha$, $c_\alpha \equiv \cos\theta_\alpha$, $(\alpha = 1, 2, 3)$ [17]. We can factor the CKM matrix as an Eulerian construction of three rotation matrices and a phase matrix,

$$V = \begin{pmatrix} 1 & 0 & 0 \\ 0 & c_2 & -s_2 \\ 0 & s_2 & c_2 \end{pmatrix} \begin{pmatrix} c_1 & -s_1 & 0 \\ s_1 & c_1 & 0 \\ 0 & 0 & 1 \end{pmatrix} \begin{pmatrix} 1 & 0 & 0 \\ 0 & 1 & 0 \\ 0 & 0 & -e^{i\delta} \end{pmatrix} \begin{pmatrix} 1 & 0 & 0 \\ 0 & c_3 & s_3 \\ 0 & -s_3 & c_3 \end{pmatrix}, \tag{2.25}$$

where $c_i = \cos\theta_i, s_i = \sin\theta_i$, or

$$V = \begin{pmatrix} c_1 & -s_1c_3 & -s_1s_3 \\ s_1c_2 & c_1c_2c_3 - s_2s_3e^{i\delta} & c_1c_2c_3 + s_2s_3e^{i\delta} \\ s_1s_2 & c_1s_2c_3 + c_2s_3e^{i\delta} & c_1s_2s_3 - c_2c_3e^{i\delta} \end{pmatrix}. \tag{2.26}$$

The CKM matrix is unitary, but if there are four, instead of three generations of quarks, the mixing of the first three generations would not be unitary by itself, a possible signature of a new generation of quarks. Among different elements of the CKM matrix, the one we focus on is V_{cb}. It multiplies the vector current $b\gamma_\mu c$, and governs the transition rate from the bottom quark to the charm quark. This is a semileptonic process as shown in the Feynman diagram 2.2. $|V_{cb}|$ appears in the amplitude of this diagram, depicted by the vertex of $b \to c$ transition.

2.4 Approximations

In this section, we will introduce some effective field theories that approximate the standard model in special cases. We will discuss two effective theories, one, chiral perturbation theory, and the other, heavy quark effective theory. Chiral perturbation theory is the effective theory which describes low energy QCD phenomena, while heavy quark effective theory describes the physics at large quark masses $m_Q \gg \Lambda_{QCD}$. Here, the QCD scale Λ_{QCD} is about 300-400 MeV.

2.4.1 Chiral perturbation theory

We give a brief introduction to continuum chiral perturbation theory [18] so that we will be able to make use of it for analyzing lattice QCD data for the semileptonic decay process. We will discuss how to implement chiral perturbation theory for $B \to Dl\nu$ process after we introduce both chiral perturbation theory and heavy quark effective theory.

2.4.2 Chiral symmetry

The fermion part of the QCD Lagrangian for the three lightest flavors u, d, and s can be written as:

$$\mathcal{L}_F = \overline{q}_L \not{D} q_L + \overline{q}_R \not{D} q_R + \overline{q}_L M q_R + \overline{q}_R M^\dagger q_L \ . \tag{2.27}$$

Here,

$$\begin{aligned} q_{L,R} &= \frac{1}{2}(1 \mp \gamma_5) q \\ M &= \begin{pmatrix} m_u & 0 & 0 \\ 0 & m_d & 0 \\ 0 & 0 & m_s \end{pmatrix} \ . \end{aligned} \tag{2.28}$$

The transformation rule of the quark field, under the chiral symmetry group $U(3)_L \times U(3)_R$ is:

$$\begin{aligned} q_{L,R} &\rightarrow U_{L,R} q_{L,R} \ , \\ \overline{q}_{L,R} &\rightarrow \overline{q}_{L,R} U^\dagger_{L,R} \ . \end{aligned} \tag{2.29}$$

The "chiral symmetry" represents the fact that the Lagrangian (2.27) is invariant under the transformation in Equation (2.29), if $M = 0$. Since the u and d quarks have small mass, and the s quark mass is fairly small, we can treat their masses as a purtubation. The chiral group is spontaneously broken to the diagonal subgroup as a vector: $SU(3)_L \times SU(3)_R \rightarrow SU(3)_V$. The order parameter for symmetry breaking is the normalized condensate,

$$\Omega_{ij} = \langle \overline{q}_{Ri} q_{Lj} \rangle = \langle \overline{q}_{Li} q_{Rj} \rangle \propto \Lambda^3_{QCD} \delta_{ij} \ . \tag{2.30}$$

This order parameter of spontaneous symmetry meaing transforms under the chiral group as $\Omega \rightarrow U_L \Omega U^\dagger_R$.

A consequence of spontaneously symmetry weaking is that there are eight pseudoscalar Nambu-Goldstone bosons. With three flavors u, d, s, the psedudoscalar mesons form an octet. This can be understood through the definition of mesons, the bound state of a quark and antiquark:

$$\phi = \begin{pmatrix} \frac{\pi_0}{\sqrt{2}} + \frac{\eta}{\sqrt{6}} & \pi^+ & K^+ \\ \pi^- & -\frac{\pi_0}{\sqrt{2}} + \frac{\eta}{\sqrt{6}} & K^0 \\ K^- & \overline{K}^0 & -\frac{2\eta}{\sqrt{6}} \end{pmatrix} \sim \begin{pmatrix} u\overline{u} & u\overline{d} & u\overline{s} \\ d\overline{u} & d\overline{d} & d\overline{s} \\ s\overline{u} & s\overline{d} & s\overline{s} \end{pmatrix} \ . \tag{2.31}$$

Since the strange quark has a larger mass than the up and down quark, it is common to restrict the model to two light flavors, with symmetry $SU(2)_L \times SU(2)_R$. ϕ then reduces to a 2×2 matrix:

$$M = \begin{pmatrix} \pi^0/\sqrt{2} & \pi^+ \\ \pi^- & -\pi^0/\sqrt{2} \end{pmatrix} \ . \tag{2.32}$$

No matter in $SU(2)$ or $SU(3)$, we will make use of ϕ to define the chial Lagrangian, which is useful in my analysis of the lattice data.

2.4.3 The chiral Lagrangian

The effective chiral Lagrangian can be written in linear and nonlinear form. We present the nonlinear form. It is written in terms of Σ, which transforms as follow:

$$\Sigma = \exp(2i\phi/f) \to U_L \Sigma U_R^\dagger \ . \tag{2.33}$$

Here, the decay constant f is of order 100 MeV. This definition is very convenient, especially when one is interested in the interaction between the pion and other mesons, such as the B and D mesons. The effective chiral Lagrangian is built from the most general terms satisfying the correct Lorentz symmetry and chiral symmetry:

$$\mathcal{L}_{eff} = \frac{1}{8} f^2 \,\mathrm{Tr}(\partial_\mu \Sigma^\dagger \partial_\mu \Sigma) + \lambda \,\mathrm{Tr}(m_q \Sigma + m_q^\dagger \Sigma^\dagger) + \cdots \ . \tag{2.34}$$

Since QCD has the same symmetry, QCD must take this form at low energy. The dots represent terms with higher derivatives. The perturbation expansion is done in terms of powers of the momentum with $\partial_\mu \leftrightarrow p_\mu$, parameterized as p/Λ_χ where Λ_χ should be at order of mass of ρ, which is 770 MeV. So we drop higher order terms at very low momentum.

2.4.4 Heavy quark effective theory with chiral perturbation theory

Both heavy quark symmetry and chiral perturbation theory are components of the effective theory of meson. Here, we introduce them in more detail.

2.4.4.1 Heavy quark symmetry

It is pointed out that the hadronic system containing a single heavy quark ($m \gg \Lambda_{QCD}$) admits additional symmetries not presented in the QCD Lagrangian [19]. Such a system is viewed as a freely propagating point-like color source, dressed by strongly interacting eight quarks and gluons, carrying appropriate color, flavor, baryon number, energy, angular momentum, and parity to make up the observed physical state. Since an infinitely massive heavy quark does not recoil from the emission and absorption of soft gluons, and since the magnetic interaction of such a quark falls off as $1/m$ and is hence negligible, neither its mass nor its spin affects the state of the light degrees of freedom. The decay of the heavy quark occurs through the action of some external current and is calculable in perturbation theory, expanding as a series in Λ_{QCD}/m. The soft interactions must be treated nonperturbatively,

so in heavy quark effective theory, they are parameterized by unknown functions, but they are independent of the mass and spins of the initial and final heavy quarks.

The typical momentum transfer Δp between the heavy and light quarks in the meson arising from nonperturbative QCD dynamics is of the order of Λ_{QCD}. So heavy quark effective theory applies when $\triangle v \equiv \triangle p/m_Q \simeq \Lambda_{QCD}/m_Q \ll 1$. Under heavy quark flavor symmetry, the dynamics is unchanged under the exchange of heavy quark flavors. In the $m_Q \to \infty$ limit, the static heavy quark can interact with gluons only via its chromoelectric charge. This interaction is spin independent. This leads to heavy quark spin symmetry: the dynamics is unchanged under arbitrary rotations of the spin of the heavy quark. The spin-dependent interactions are proportional to the chromomagnetic moment of the quark, and so are of the order of Λ_{QCD}/m_Q. For a heavy quark with N_h heavy quark flavors, one may build a large symmetry group to describe the heavy-light system containing such a heavy quark. Such a group is the $U(2N_h)$ spin-flavor symmetry group. We then will be able to use such a property to build up the effective theory of heavy quark interaction.

Under heavy quark symmetry, we set the velocity of an on-shell quark to $v = p/m_Q$. The momentum of an off-shell quark can be written as $p = m_Q v + k$. We then can write the simplified Dirac quark propagator as:

$$i\frac{1+\not{v}}{2v\cdot k + i\epsilon} \ . \tag{2.35}$$

We then try to assemble the effective Lagrangian in terms of the velocity-dependent field $Q_v(x)$:

$$Q(x) = e^{-im_Q v\cdot x}[Q_v(x) + \mathcal{V}_v(x)] \ . \tag{2.36}$$

Here, we have:

$$\begin{aligned} Q_v(x) &= e^{im_Q v\cdot x}\frac{1+\not{v}}{2}Q(x) \ , \\ \mathcal{V}_v(x) &= e^{im_Q v\cdot x}\frac{1-\not{v}}{2}Q(x) \ . \end{aligned} \tag{2.37}$$

We then can write the effective Lagrangian at leading order in $1/m_Q$ as follows:

$$\mathcal{L}_{eff} = \sum_{i=1}^{N_h}\overline{Q}_v^{(i)}(iv\cdot D)Q_v^{(i)} \ . \tag{2.38}$$

Here, N_h is the number of heavy quark flavors, and all the heavy quarks have the same four-velocity v. With these basics of heavy quark effective theory, we are ready to look at the application of chiral perturbation theory and heavy quark effective theory.

2.4.4.2 Chiral perturbation theory for semileptonic form factors

We can define the doublet for spin-zero and spin-one mesons, denoted as P_a and P_a^* [20] where the a labels the light quark q_a. So $a = 1, 2$ and $q_1 = u, q_2 = d$. Meanwhile, P_a denotes the spin-zero mesons and P_a^* denotes the spin-one mesons. For the semileptonic decays $B \to D^{(*)}$, we have two cases. For case $Q = c$, we have $P_a = (D^0, D^+)$ and $P_a^* = (D^{*0}, D^{*+})$, while for case Q=b, we have $P_a = (B^-, B^0)$ and $P_a^* = (B^{*-}, B^{*0})$. For convenience of establishment of the effective theory, we define the 4×4 matrix H_a as follows:

$$H_a = \left(\frac{1+\not{v}}{2}\right)(P^*_{a\mu}\gamma^\mu - P_a\gamma_5) \ . \tag{2.39}$$

We also define $\overline{H}_a = \gamma^0 H_a^\dagger \gamma^0$. To include interaction with mesons, we define $\xi = \exp(iM/f)$, where M is defined in Equation (2.32). We then can build the Lagrange density based on the chiral symmetry $SU(2)_L \times SU(2)_R$ as follows:

$$\begin{aligned} \mathcal{L} = \ & - \ i \,\mathrm{Tr}\,\overline{H_a} v_\mu \partial^\mu H_a + \frac{1}{2} i \,\mathrm{Tr}\,\overline{H}_a H_b v^\mu (\xi^\dagger \partial_\mu \xi + \xi \partial_\mu \xi^\dagger)_{ba} \\ & + \ \frac{1}{2} ig \,\mathrm{Tr}\,\overline{H}_a \gamma_\nu \gamma_5 H_b (\xi^\dagger \partial^\nu \xi - \xi \partial^\nu \xi^\dagger)_{ba} + \cdots \ . \end{aligned} \tag{2.40}$$

In perturbation theory, a term proportional to $1/m_Q$ will give rise to a logarithm term in a one-loop calculation. The loop diagram is shown in Figure 2.3. This term is :

$$\delta\mathcal{L}^{(2)} = \frac{\lambda_2}{m_Q} \,\mathrm{Tr}\,\overline{H}_a \sigma^{\mu\nu} H_a \sigma_{\mu\nu} \ . \tag{2.41}$$

The λ_2 here generate the mass splitting $\Delta^{(Q)} = m_{P^*(Q)} - m_{P(Q)}$, one of the quantites that I use in my data analysis. For $B \to Dl\nu$ process, the vector current $\mathcal{V}_{cb}$ can be written in heavy quark effective theory as:

$$\mathcal{V}_{cb} = \bar{c}\Gamma b = -\beta(w) Tr \overline{H}_a^{(c)}(v')\Gamma H_a^b(v) + \cdots \ , \tag{2.42}$$

where $\Gamma_\mu = \gamma_\mu$ or $\Gamma_\mu = \gamma_\mu\gamma_5$, corresponding to $B \to Dl\nu$ and $B \to D^* l\nu$.

In our formalism, we write the form factors in chiral perturbation theory as a tree level term plus a one loop logarithmic term. From heavy quark theory calculation, the tree level h_+ at zero recoil is 1, and h_- at treelevel is 0. The one loop correction shown in Figure 2.3 provide us a logarithm term.

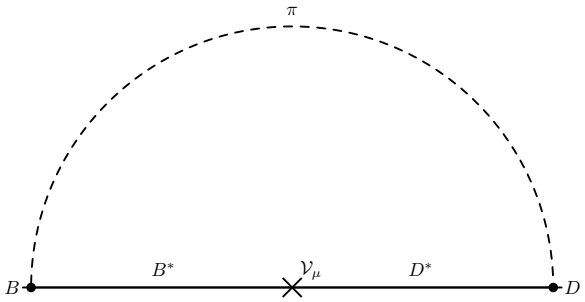

Figure 2.3. One loop diagram in heavy quark chiral perturbation theory for the vector current in $B \to Dl\nu$ in heavy quark chiral perturbation on theory modifying the vector current. The dotted line is the pion in the $DD^*\pi$ interaction, linking with the vertex of $DD^*\pi$ and the vertex of $BB^*\pi$. The cross is the insertion of weak interaction vertex, which corresponds to the transition from b quark to c quark.

As will be introduced in the next chapter, the vector current can be parameterized with Lorentz invariant form factors h_+ and h_-. So this loop calculation gives a correction to these form factors. The correction for h_- is 0, while the correction for h_+ is:

$$\begin{aligned} \delta h_+ &= \frac{3ig^2\beta}{f^2}[(w+2)I_1(\Delta,w) + (w^2-1)I_2(\Delta,w) \\ &\quad -\frac{3}{2}I_3(\Delta,w) - \frac{3}{2}I_3(0,2)] \ . \end{aligned} \tag{2.43}$$

Here, I_i ($i \in \{1,2,3\}$) denotes as the integrals as follow:

$$\begin{aligned} I_1 &= \mu^{4-n}\int_0^\infty d\alpha \int_0^\infty d\beta \int \frac{d^nk}{(2\pi)^n} \frac{k^2}{[k^2-(\alpha^2+\beta^2+2\alpha\beta w+2\Delta\alpha+m_\pi^2)+i\epsilon]^3} \ , \\ I_2 &= 4\mu^{4-n}\int_0^\infty d\alpha \int_0^\infty d\beta \int \frac{d^nk}{(2\pi)^n} \frac{\alpha\beta}{[k^2-(\alpha^2+\beta^2+2\alpha\beta w+2\Delta\alpha+m_\pi^2)+i\epsilon]^3} \ , \\ I_3 &= \mu^{4-n}\int_0^\infty d\alpha \int_0^\infty d\beta \int \frac{d^nk}{(2\pi)^n} \frac{\alpha k^2}{[k^2-(\alpha^2+2\Delta\alpha+m_\pi^2)+i\epsilon]^3} \ . \end{aligned} \tag{2.44}$$

So here, μ is the subtraction point required by the renormalization theory, and $\delta = m_{D^*} - m_D$ is the mass splitting of D and D^* mesons. These integrals lead to the logarithm term given in the Appendix and [21]. Those expressions also include modification needed for our staggered fermion action for lattice (staggered χPT) discussed in Chapter 4.

CHAPTER 3

PHENOMENOLOGICAL BACKGROUND OF THIS WORK

The purpose of this chapter is to give an overview of the phenomenological background of the semileptonic decay $B \to Dl\nu$ and the CKM matrix. We explain the need for a precise determination of $|V_{cb}|$.

3.1 Unitarity triangle

The unitary property of the CKM matrix leads to constraints on the complex matrix element; for example:

$$\begin{aligned} V_{ub}^* V_{ud} + V_{cb}^* V_{cd} + V_{tb}^* V_{td} &= 0 \ , \\ \frac{V_{ub}^* V_{ud}}{V_{cb}^* V_{cd}} + 1 + \frac{V_{tb}^* V_{td}}{V_{cb}^* V_{cd}} &= 0 \ . \end{aligned} \tag{3.1}$$

These three complex numbers sum to form a triangle in the complex plane. For this reason, we call it the "unitary triangle."

3.1.1 Parameterization of CKM matrix

The CKM matrix elements vary strongly in magnitude with the largest ones on the diagonal and smallest off the diagonal. So Wolfenstein introduced a convenient approximate parameterization that incorporates this observation. The element V_{us} is well known, $\lambda \approx |V_{us}| \approx 0.22$. Since $|V_{cb}|$ is about 0.04, *i.e.,* it is of order λ^2, we set $V_{cb} = A\lambda^2$, and so on.

With the same notation in Equation (2.25), we have the following definition:

$$\begin{aligned} \lambda &= s_1 \ , \\ A\lambda^2 &= (s_2^2 + s_3^2 + 2 s_2 s_3 \cos\delta)^{1/2} \ , \\ A^2\lambda^4\eta &= s_2 s_3 \sin\delta \ , \\ A\lambda^2(\rho^2+\eta^2)^{1/2} &= s_3 \ . \end{aligned} \tag{3.2}$$

With these definitions and Equation (2.26), the various CKM matrix elements can be expanded as the Taylor expansion of λ. One just needs to compute the cosine values

according to the sine values, and insert into Equation (2.26). Up to $\mathcal{O}(\lambda^4)$, we get the Wolfenstein approximation:

$$\begin{aligned} V &= \begin{pmatrix} V_{ud} & V_{us} & V_{ub} \\ V_{cd} & V_{cs} & V_{cb} \\ V_{td} & V_{ts} & V_{tb} \end{pmatrix} \\ &= \begin{pmatrix} 1-\lambda^2/2 & \lambda & \lambda^3 A(\rho - i\eta(1-\lambda^2/2)) \\ -\lambda & 1-\lambda^2/2 - i\eta A^2\lambda^4 & \lambda^2 A(1+i\eta\lambda^2) \\ \lambda^3 A(1-\rho-i\eta) & -\lambda^2 A & 1 \end{pmatrix} . \end{aligned} \tag{3.3}$$

To lowest order in λ^2, we have:

$$\rho + i\eta \approx -\frac{V_{ud}V_{ub}^*}{V_{cd}V_{cb}*} . \tag{3.4}$$

To higher order, we define:

$$\overline{\rho} + i\overline{\eta} = -\frac{V_{ud}V_{ub}^*}{V_{cd}V_{cb}*} . \tag{3.5}$$

For example, we get V_{ud} as follows:

$$V_{ud} = 1 - \frac{1}{2}\lambda^2 - \frac{1}{8}\lambda^4 - \frac{1}{16}\lambda^6(1+8A^2(\rho^2+\eta^2)) - \frac{1}{128}\lambda^8(5-32A^2(\rho^2+\eta^2)) , \tag{3.6}$$

and get:

$$\begin{aligned} \overline{\rho} &= \rho(1-\frac{\lambda^2}{2}) + (\frac{1}{2}A^2\rho - \frac{1}{8}\rho - A^2(\rho^2-\eta^2))\lambda^4 + \mathcal{O}(\lambda^6) \\ \overline{\eta} &= \eta(1-\frac{\lambda^2}{2}) + (\frac{1}{2}A^2\eta - \frac{1}{8}\eta - 2A^2\rho\eta)\lambda^4 + \mathcal{O}(\lambda^6) . \end{aligned} \tag{3.7}$$

3.2 Determination of unitarity triangle

In this section, we show how theory and experiment constrain the unitarity triangle. Various physical quantities are fit simultaneously to determine the apex of this triangle. This is called the UT fit, or global fit, as shown in Figure 3.1. The bands in Figure 3.1 represent the one sigma range of uncertainty in the constraints. These physical quantities are $|\epsilon_k|$, $\triangle M_{B_d}$, $\triangle M_{B_s}$, $\sin 2\beta$, γ, and $\sin\alpha$ [17]. We introduce them one by one.

3.2.1 $|\varepsilon_K|$

The neutral kaon system provides constraints on the unitarity triangle through $K^0\overline{K}^0$ mixing and direct CP violation. ε_K is one of the CP-violation parameters. As mentioned in [22], ε_K in the Wolfstein parameterization, is:

$$\begin{aligned} \varepsilon_K &= C_\epsilon \widehat{B}_K A^2\lambda^6\overline{\eta}\Big\{ -\eta_1 S_0(x_c)(1-\frac{\lambda^2}{2}) \\ &\quad +\eta_3 S_0(x_c,x_t) + \eta_2 S_0(x_t)A^2\lambda^4(1-\overline{\rho})\Big\} . \end{aligned} \tag{3.8}$$

Here, $C_\epsilon = G_F^2 f_K^2 M_K M_W^2/(6\sqrt{2}\pi^2\triangle m_K)$, where S_0 is an Inami-Lim function, $x_q^2 = m_q^2/m_W^2$, and η_i are perturbative QCD corrections. f_K is the neutral kaon decay constant, about

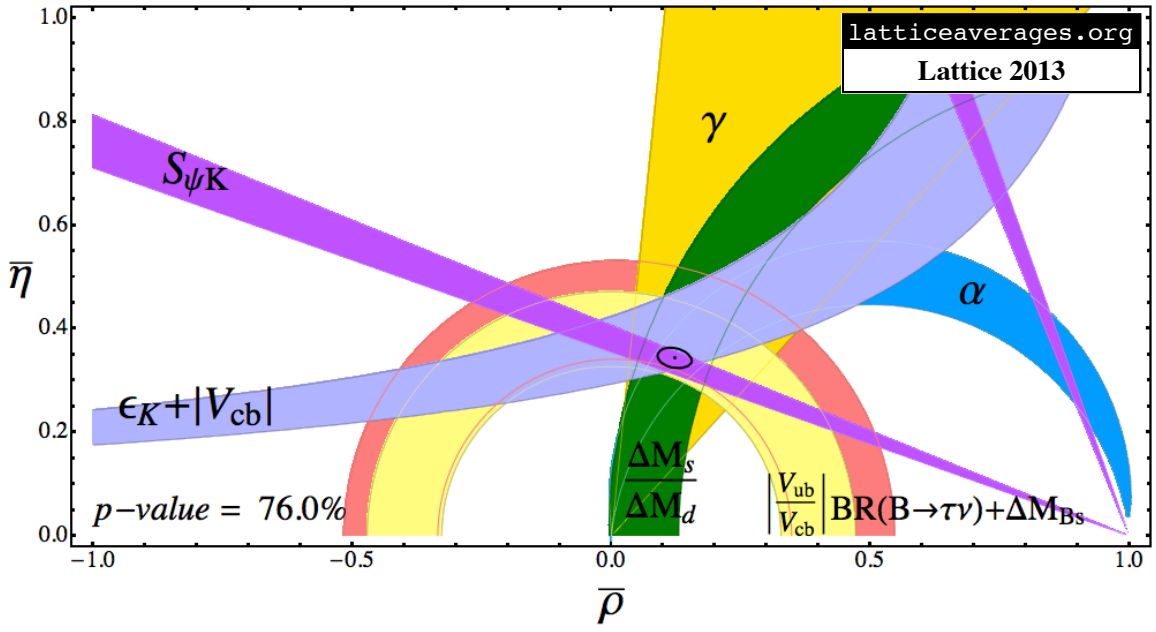

Figure 3.1. Unitary triangle fit using the standard model [1].

160MeV. $\widehat{B}_K$ is the "bag parameter," which is related the hadronic matrix element for $K\overline{K}$ mixing through:

$$\langle \overline{K}^0 | (\bar{s}\gamma^\mu(1-\gamma^5)d)^2 | K^0 \rangle = \frac{8}{3} m_K^2 f_K^2 B_K \ . \tag{3.9}$$

$\widehat{B}_K$ contains the nonperturbative QCD contributions for ε_K, and is determined by lattice QCD. It is measured to be about 1. So the value of ε_K is bounded by approximate hyperboles. The main error is due to the bag parameter. There is also a parametric uncertainty proportional to the fourth order of A, one of the Wolfstein parameters. The source of this error is the value of $(V_{ts}V_{td}^*)^2$, which is approximately $\sigma(|V_{cb}^4|)$. So we see that the uncertainty of V_{cb} also plays a role in the determination of ε_K.

3.2.2 ΔM_{B_d}

ΔM_{B_d}, also denoted as Δm_d, is the so-called *mixing frequency* or *oscillation frequency* of B_d. It is defined as the mass difference between B_d and $\overline{B_d}$, two different mass eigenstates. This quantity is driven by the effective flavor-changing neutral-current process through $\delta B = 2$ box diagrams, as shown in Figure 3.2. This kind of diagram is dominated by top quark exchange between the virtual $W^\pm$ boson lines.

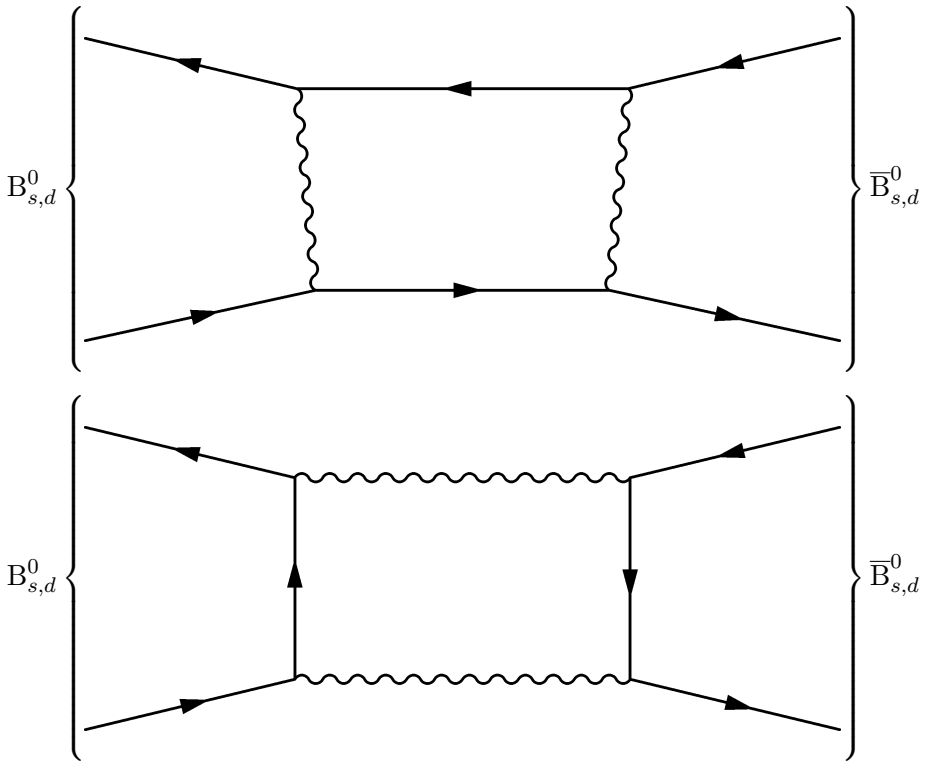

Figure 3.2. Box diagram of $B\overline{B}$ mixing. [2]

3.2.3 ΔM_{B_s}

ΔM_{B_s}, also denoted as Δm_s, is the mixing frequency of B_s, or the mass difference of B_s and $\overline{B_s}$.

3.2.4 $\sin 2\beta$

The parameter β is defined as follows:

$$\beta = \arg\left[-\frac{V_{cd}V_{cb}^*}{V_{td}V_{tb}^*} \right] . \tag{3.10}$$

As an approximation, $\sin 2\beta$ is equal to the time-dependent CP-violation parameter S in the $b \to c\bar{c}s$ process. An example of such a process is $B \to J/\psi K_s$. Here, β is the phase of V_{td}^*.

3.2.5 γ

The parameter γ is defined as follows:

$$\gamma = arg\left[-\frac{V_{ud}V_{ub}^*}{V_{cd}V_{cb}^*} \right] . \tag{3.11}$$

This parameter is measured from the process $B \to D^{(*)}K^{(*)}$.

3.2.6 $\sin\alpha$

The parameter α is defined as follow:

$$\alpha = \arg\left[-\frac{V_{td}V_{tb}^*}{V_{ud}V_{ub}^*} \right] . \tag{3.12}$$

It is determined from time-dependent CP asymmetries in the process $B \to (\pi\pi, \rho\rho, \rho\pi)$.

3.2.7 $|V_{ub}|/|V_{cb}|$

The parameter $|V_{ub}|$ is determined from the semileptonic decay $B \to \pi l\nu$ and the leptonic decay $B \to \tau\nu$. The parameter $|V_{cb}|$ is determined from $B \to Dl\nu$ in this thesis and $B \to D^*l\nu$. Since the $B \to \tau\nu$ determination of $|V_{ub}|$ gives a slightly different result, it is shown separately in Figure 3.1. If the standard model is correct, all bands in the unitarity triangle must intersect at a common apex. They don't quite. The p value of the global unitary triangle fit is approximately 76%. This happens partly because of the disagreement between the determination of $|V_{ub}|$ from $B \to \tau\nu$ and $B \to \pi l\nu$. Then, as we mentioned in Chapter 1, there is a 2σ difference between the inclusive and exclusive determination of V_{cb} in the decays $B \to Dl\nu$ and $B \to D^*l\nu$.

3.3 Measuring the decay rate of $B \to Dl\nu$

The form factors $f_+(w)$ can be measured by experiment. Here, we give a brief explanation of how the semileptonic decay is measured. Take the BABAR detector [23] as an example. It was at the standard Linear AcceleratorPEP-II, ring asymmetric collider. The center of mass of the colliding e^+e^- moves with velocity $\beta = 0.49$ along the beam axis in the laboratory rest frame. The data collected at energies near the peak of the $\Upsilon(4S)$ resonance correspond to $B\overline{B}$ decays. Data collected just below the $B\overline{B}$ threshold are used to subtract the $e^+e^- \to q\overline{q}(q = u, d, s, c)$ background under the $\Upsilon(4S)$ resonance. So there is a good sample of B and B^* mesons. The measurable quantities in experiment are the momenta of the charged leptons (electron or muon) and longer lived decay products. Since the D meson has a very short lifetime, it can not be measured directly. However, the D meson decay products can be measured. A typical event leading to observable particles is

$$\begin{aligned} \overline{B}^{-1} &\to D^0 e^- \overline{\nu}_e \ , \\ D^0 &\to K^0\pi \ , \\ \pi^0 &\to \gamma\gamma \ . \end{aligned} \tag{3.13}$$

Here, the electron, kaon, and two photons are observed and the neutrino is inferred from energy and momentum conservation. We discuss here how the form factors are related to the differential decay rate of $B \to Dl\nu$ process.

To extract the hadronic form factor, we start from the hadronic matrix element. The form factors are parameterized so that the Lorentz transformation property is preserved. The hadronic matrix element of the vector current of the b to c transition is parameterized with form factors f_+ and f_0 as follows:

$$\begin{aligned}\langle D(p')|\mathcal{V}|B(p)\rangle &= f_+(q^2)\left[(p+p')^\mu - \frac{M_B^2 - M_D^2}{q^2}q^\mu\right] \\ &\quad + f_0(q^2)\frac{M_B^2 - M_D^2}{q^2}q^\mu \ . \end{aligned} \tag{3.14}$$

Here, $\mathcal{V}^\mu = \bar{b}\Gamma^\mu c$ is b to c vector current. p and p' are the momenta of the B and D mesons, respectively. M_B and M_D are the masses of the B and D mesons. $q^2 = (p-p')^2$ is the momentum transfer. When $q^2 = 0$, we have the kinematic constraint, namely $f_+(0) = f_0(0)$.

Alternative form factors h_+ and h_- are also used:

$$\frac{\langle D(p')|\mathcal{V}^\mu|B(p)\rangle}{\sqrt{M_B M_D}} = h_+(w)(v+v')^\mu + h_-(w)(v-v')^\mu \ . \tag{3.15}$$

They are linearly related to f_+ and f_0 is as follows:

$$\begin{aligned} f_+(w) &= \frac{1}{2\sqrt{r}}[(1+r)h_+(w) - (1-r)h_-(w)] \\ f_0(w) &= \sqrt{r}\left[\frac{w+1}{1+r}h_+(w) - \frac{w-1}{1-r}h_-(w)\right] \ . \end{aligned} \tag{3.16}$$

Here, we have defined $r = M_D/M_B$ and $w = v \cdot v'$, the velocity transfer, where $v = p_B/M_B$, and $v' = p_D/M_D$, The velocity transfer w is related to the invariant momentum transfer through $q^2 = M_B^2 + M_D^2 - 2wM_BM_D$. So the form factors can be regarded as functions of w. Note that $w = 1$ implies zero recoil ($v = v'$), which corresponds to $q^2 = (3.41\text{eV})^2$.

The amplitude corresponding to Figure 2.2 of the $B \to D$ decay is as what we discussed in Equation (2.24). Making use of the amplitude, we can construct the decay rate as follows:

$$d\Gamma = \frac{2\pi}{2m_B}|\mathcal{A}|^2 d\phi_f \ . \tag{3.17}$$

where we have:

$$d\phi_f(p', p_l, p_\nu) = (2\pi)^4\delta^{(4)}(p' + p_l + p_\nu - p) \times \frac{1}{(2\pi)^6}\frac{d^3p'}{2E'}\frac{d^3p_l}{2E_l}\frac{d^3p_\nu}{2E_\nu} \ . \tag{3.18}$$

Here, p' is the momentum of D meson, p is the momentum of B meson, p_l is the momentum of electron or muon, and p_ν is the momentum of nutrino.

Without any approximation on the lepton mass, after integrating, we get the following result:

$$\frac{d\Gamma}{dq^2} = \frac{G_F^2|V_{cb}|^2}{24\pi^3}|p'|^3(1-2\rho)^2\left\{(1+\rho)|f_+(q^2)|^2 + 3\rho|f_0'(q^2)|^2\right\} . \tag{3.19}$$

Here, $\rho = m_l^2/2q^2$ and $f_0'(q^2) = [(M_B^2 - M_D^2)f_+(q^2) + 3\rho|f_0(q^2)|^2]/(2M_B|p'|)$.

For this thesis, since the mass of electron or muon is very small compared with $M_B - M_D$, we set $m_l = 0$, and get the following result:

$$\frac{d\Gamma}{dw}(\overline{B} \to Dl\overline{\nu_l}) = \frac{G_F^2|V_{cb}|^2 m_B^5}{48\pi^3}(w^2-1)^{3/2}r^3(1+r)^2\mathcal{G}_D(w)^2 . \tag{3.20}$$

where

$$\mathcal{G}_D(w)^2 = \left[h_+ + \left(\frac{1-r}{1+r}\right)h_-\right]^2 \tag{3.21}$$

and

$$|f_+(w)|^2 = \frac{(1+r)^2}{4r}\mathcal{G}_D(w)^2 . \tag{3.22}$$

So the differential decay rate is proportional to the square of only the form factor f_+.

CHAPTER 4

INTRODUCTION TO LATTICE GAUGE THEORY

This research is based on lattice gauge theory. So we provide an introduction to the basics of lattice gauge theory.

4.1 Feynman path integral

Since the numerical simulation of lattice field theory is defined in the framework of the Feynman path integral, the theory which connects classical mechanics with quantum mechanics, we need first to introduce the Feynman path integral [24].

The Feynman path integral is an integration over classical time histories. We use the simple example of a quantum mechanical path integral to show how we discretize the path integral. We first consider the Green function, or propagator, for a particle moving from position x_i at time t_i to position x_f at time t_f. It is given by the Feynman path integral:

$$G(x_f, t_f; x_i, t_i) = \langle x_f | e^{-i\widehat{H}(t_f - t_i)} | x_i \rangle = \int \mathcal{D}x(t) e^{-iS[x]} \ . \tag{4.1}$$

The integration with measure $\mathcal{D}x(t)$ is a sum over all possible particle paths. The classical action is:

$$S[x] \equiv \int_{t_i}^{t_f} dt L(x, \dot{x}) \equiv \int_{t_i}^{t_f} dt \left[\frac{m\dot{x}(t)^2}{2} - V(x(t)) \right] \ . \tag{4.2}$$

Then, to discretize the path integral, we specify $x(t)$ only on the nodes or sites of a discretized t axis:

$$\begin{aligned} t_j &= t_i + ja \\ T &= t_f - t_i = Na \end{aligned} \tag{4.3}$$

for $j = 0, 1 \cdots N$. We then have a vector:

$$x = \{x(t_0), x(t_1) \cdots x(t_N)\} \ . \tag{4.4}$$

We refer to such a path as a "configuration." With these definitions, we get the lattice version of the propagator:

$$\langle x|e^{-i\hat{H}T}|x\rangle \approx A\int_{-\infty}^{\infty} dx_1\cdots dx_{N-1}e^{-iS_{lat}[x]}\ . \tag{4.5}$$

The lattice action is:

$$S_{lat}[x] \equiv \sum_{j=0}^{N-1}\left[\frac{m}{2a}(x_{j+1}-x_j)^2 - aV(x_j)\right]\ . \tag{4.6}$$

We then can use a simulation method, such as Monte Carlo, to evaluate the integral.

The path integral formalism also provides a method for evaluating expectation values of operators on a quantum thermal ensemble or on the ground state (vacuum) in the limit of zero temperature. In this case, we want to evaluate:

$$\langle\Gamma\rangle = \frac{\mathrm{Tr}\,\Gamma e^{-H/kT}}{\mathrm{Tr}\,e^{-H/kT}} \tag{4.7}$$

We get this expectation value from Equation (4.2) by setting $x_i = x_f \equiv x$ and $(t_f - t_i) = 1/kT$, and integrate over x. Thus we go to imaginary time. In this case, the action $S[x]$ will be a sum of the kinematic and potential. We get:

$$\langle\gamma[x]\rangle = A\int_{-\infty}^{\infty} dx dx_1\cdots dx_{N-1}e^{-S[x]} \tag{4.8}$$

The ground state expectation value is obtained by taking $kT \to 0$ or $(t_f - t_i) \to \infty$. That is the method used in this thesis.

We can generate a large number, N_{cf}, of random configuration (paths), with probability weight $e^{-S(x)}$ as follows:

$$x^{(\alpha)} \equiv x_0^{(\alpha)}x_1^{(\alpha)}\cdots x_{N-1}^{(\alpha)} \tag{4.9}$$

with $\alpha = 1, 2\cdots N_{cf}$. If the probability $P[x^{(\alpha)}]$ to obtain the path $x^{(a)}$ is proportional to $e^{-S[x]}$, then the desired expectation value is the simple average of the value on each configuration.

$$\langle\Gamma([x])\rangle \approx \frac{1}{N_{cf}}\sum_{\alpha=1}^{N_{cf}}\Gamma[x^{(\alpha)}]\ . \tag{4.10}$$

4.2 QCD on lattice

We start from the Lagrangian density of the continuum theory of QCD, and modify it to get lattice Lagrangian of QCD.

4.2.1 Setup of lattice QCD

For lattice simulation of QCD, we need to discretize both space and time [25]. So for the $3+1$ space-time, we have a hypercubic lattice with lattice spacing a. Lattice QCD is established in such a way that the lattice action finally reduces to the continuum action in the limit $a \to 0$. One begins by defining the link: matrix connecting site x with the neighboring site $x + a\hat{\mu}$ where $\hat{\mu}$ is a unit vector along the μ direction. The link $U_\mu(x)$ is:

$$U_\mu(x) \equiv \mathcal{P} \exp\left(-i \int_x^{x+a\widehat{\mu}} gA \cdot dy \right) . \tag{4.11}$$

Here, the color vector potential field A is $A_\mu^a \lambda^a$, with $\lambda_a (a = 1, 2, 3)$, the eight generators of $SU(3)$ group. g is the gauge coupling constant.

We then consider the plaquette constructed from four links of a unit square in the μ, ν plane:

$$P_{\mu\nu}(x) \equiv \frac{1}{3} \operatorname{Re} \operatorname{Tr}(U_\mu(x) U_\nu(x + a\widehat{\mu}) U_\mu^\dagger(x + a\widehat{\mu} + a\widehat{\nu}) U_\nu^\dagger(x)) . \tag{4.12}$$

Using the Baker–Campbell–Hausdorff Theorem and Stoke's Theorem, we can expand the plaquette operator as:

$$\begin{aligned} P_{\mu\nu} &= 1 - c_1 a^4 \operatorname{Tr}(g F_{\mu\nu}(x_0)^2) \\ &\quad - c_2 a^6 \operatorname{Tr}(g F_{\mu\nu}(x_0)(D_\mu^2 + D_\nu^2) g F_{\mu\nu}(x_0)) + \mathcal{O}(a^8) . \end{aligned} \tag{4.13}$$

where $c_1 = 1/6$ and $c_2 = 1/72$ and $F_{\mu\nu} \equiv \partial_\mu A_\nu - \partial_\nu A_\mu + ig[A_\mu, A_\nu]$.

If we write the action for the gluon as:

$$S_W = \beta \sum_{x,\mu>\nu} (1 - P_{\mu\nu}(x)) , \tag{4.14}$$

then it reduces to $\sum_{x,\mu\nu} a^4 \operatorname{Tr} F_{\mu\nu}(x)^2$ plus corrections of order a^2 as $a \to 0$. Generally speaking, $\beta = 2N/g^2$ for the $SU(N)$ gauge group. g^2 is the bare coupling constant. In this thesis, with $N = 3$, we have $\beta = 6/g^2$.

For the fermion part, by replacing the covariant derivative of fermion with a covariant difference, one can get the so-called *naive* action as follows:

$$S_{naive} = a^4 \sum_x \overline{\psi}(x) \left\{ \sum_\mu \gamma_\mu^E \bigtriangledown_\mu \psi(x) + m\psi(x) \right\} . \tag{4.15}$$

Here, the Euclidean gamma matrices γ_μ^E are chosen as $\gamma_4^E = \gamma^0$, $\gamma_i^E = -i\gamma^i$. We also have the covariant difference defined with the link field as follows:

$$\bigtriangledown_\mu \psi(x) = \frac{1}{2a} [U_\mu(x)\psi(x + a\widehat{\mu}) - U_\mu^\dagger(x - a\widehat{\mu})\psi(x - a\widehat{\mu})] . \tag{4.16}$$

In the continuum limit $a \to 0$, it reduces to the continuum QCD action shown in Equation (2.1)

4.2.2 Lattice path integral and fermionic determinant

The path integral on the lattice is given as follows:

$$Z(\beta) = \int \prod_{x,\mu} dU_\mu(x) \prod_x [d\overline{\psi}(x) d\psi(x)] \exp\{-S_G - S_F\} \ . \tag{4.17}$$

Here, $dU(x)$ is the invariant $SU(3)$ Haar measure and $[d\overline{\psi}(x)d\psi(x)]$ is a integral over Grassmann fields $\psi(x)$ and $\overline{\psi}(x)$.

The integration over the Grassman fields can be done immediately. It gives:

$$\int [d\overline{\psi}(x) d\psi(x)] e^{-S_F} = \det M = \exp(\mathrm{Tr} \ln M) \ . \tag{4.18}$$

In our notation, the M is the Dirac matrix. This leads to an effective action $S_{eff} = S_G - \mathrm{Tr} \ln M$ for the gluons.

4.2.3 Fermion doubling problem

For the fermion field, the inverse propagator in momentum space derived from this naive action is as follows:

$$a\mathcal{S}^{-1}(ap) = i \sum_\mu \gamma_\mu \sin(ap_\mu) + am \ . \tag{4.19}$$

So we have:

$$\sinh^2 aE = (am)^2 + \sum_{i=1}^{3} \sin^2 ap_i \ . \tag{4.20}$$

So the minimum of the right-hand side of this formula gives the doublers—8 of them for each choice of E [26]. So, the particle states occur at the zeros of $\det \mathcal{S}^{-1}(p)$ or when $(am)^2 + \sum_\mu \sin^2(ap_\mu) = 0$. But $\sin^2 ap_\mu$ has zero at $p_\mu = 0$ and $\pm\pi/a$, so we get states on all 16 corners of the Brillouin zone in a $d = 4$ hypercube. So, although we want to put only one fermion on the lattice, we actually get 16 when we take the continuum limit. This is called the fermion doubling problem.

There are various methods for solving the doubling problem. This is why we have different fermion formulations. We will introduce the Wilson action, Fermilab action, and staggered fermion action, respectively, in this chapter.

4.2.4 Wilson action

Wilson recognized the doubling problem when he first formulated the lattice gauge theory. He proposed adding an irrelevant term, which vanishes in the continuum limit $a \to 0$, resulting in the modified action:

$$S_W = S_{naive} - \frac{ar}{2} \sum_x \overline{\psi}(x) \sum_\mu \triangle_\mu \psi(x) \ . \tag{4.21}$$

Here, S_{naive} is defined in Equation (4.15). $\psi(x)$ is the fermion field on lattice. The second difference $\triangle_\mu\phi(x)$ is defined as follows:

$$\triangle_\mu\phi(x) = \frac{1}{a^2}[U_\mu(x)\phi(x+a\widehat{\mu}) + U_\mu^\dagger(x-a\widehat{\mu})\phi(x-a\widehat{\mu}) - 2\phi(x)] \ . \tag{4.22}$$

Here, one usually sets $r = 1$. So now the doublers with n momentum components π/a will get mass $m + 2nr/a$, which becomes infinite as $a \to 0$, and only one fermion with momentum approximately zero will have mass m. So the benefit of the Wilson action is that it solves the doubling problem. However, we introduce another problem, namely the chiral symmetry, introduced in section 2.4.2, is explicitly broken by this term. To solve this problem, one needs to tune the bare mass parameter and coupling constant carefully.

4.2.5 Fermilab action

The Fermilab action [27] is established for the purpose of reducing lattice artifacts. Before the Fermilab action was introduced, it was difficult to deal with a relativistic heavy quark on lattice. For example, the nonperturbatively $\mathcal{O}(a)$-improved Sheikholeslami-Wohlert (SW) or "clover" action has large lattice artifacts for heavy quarks. Nonrelativistic QCD deals with heavy quarks naturally, but it has no continuum limit. Heavy quark effective theory beyond the static limit is not accurate for nonzero recoil. The Fermilab action, on the other hand, is applicable for both $ma \ll 1$ and $ma \gg 1$. Also, there is no $\mathcal{O}(ma)$ divergent error for large quark mass. Only $\mathcal{O}(\Lambda_{QCD}a)$ remains.

For heavy quarks, such as the charm quark and bottom quark, in this thesis, we use the Fermilab action:

$$S = S_0 + S_B + S_E \tag{4.23}$$

Here, S_0 is the dimension three and four interaction:

$$\begin{aligned} S_0 &= \sum_n \overline{\Psi}_n\Psi_n - \kappa_t\sum_n\left[\overline{\Psi}_n(1-\gamma_0)U_{n,0}\Psi_{n+\widehat{0}} + \overline{\Psi}_n(1+\gamma_0)U_{n,0}^\dagger\Psi_n\right] \\ &- \kappa_s\sum_{n,i}\left[\overline{\Psi}_n(r_s-\gamma_i)U_{n,i}\Psi_{n+\widehat{i}} + \overline{\Psi}_n(r_s+\gamma_i)U_{n,i}^\dagger\Psi_n\right] \ . \end{aligned} \tag{4.24}$$

S_B is the chromomagnetic interaction:

$$S_B = \frac{i}{2}c_B\kappa_s\sum_{n;i,j,k}\epsilon_{i,j,k}\overline{\Psi}_n\sigma_{ij}B_{n;k}\Psi_n \ , \tag{4.25}$$

and similarly, the chromoelectric interaction is:

$$S_E = ic_E\kappa_s\sum_{n;i}\overline{\Psi_n}\sigma_{0i}E_{n;i}\Psi_n \ . \tag{4.26}$$

In our simulation, we used $\kappa_t = \kappa_s$ and $r_s = 1$, $c_E = c_B$, which is the same as the SW action. However, the Fermilab interpretation removes discretization errors. We then treat mass of the heavy quark using a dispersion relation as follows:

$$E(p) = m_1 + \frac{p^2}{2m_2} \ . \tag{4.27}$$

Here, m_1 is the rest mass, and m_2 is kinematic mass. Lattice discretization errors make $m_1 \neq m_2$. We make m_2 equal to mass measured in experiment. This will provide the improvement from SW action.

4.2.6 Staggered fermion action

The staggered fermion formulation uses a different method for dealing with the doubling problem. It is one of the cheapest fermion formulations, since staggered fermions have only one spin component per lattice site. Also they have a remnant chiral symmetry that insures positivity of the fermion determinant at positive quark mass. However, in order to eliminate the residual, unwanted extra tastes (corresponding to several doublers), one uses the so-called "fourth-root procedure," which is controversial.

Staggered fermions are obtained from naive fermions (introduced in previous section) by redistributing the spinor degrees of freedom across different lattice sites. As a result, staggered fermions describe a theory with four (rather than the 16 naive) degenerate fermion species, usually called "tastes" to distinguish them from real flavors. In order to obtain a theory with a single physical flavor, one usually takes the fourth root of the fermionic determinant for staggered fermions; this is correct in the free theory and in perturbation theory, and in chiral perturbation theory, but it is not proven to work at all energy scales. Still, there is a lot of circumstantial evidence that the method is correct [28].

4.2.7 Improvement of the lattice action

Improving the gauge action reduces lattice artifacts. Figure 4.1 shows the improvement terms of gluon action developed by Lücher-Weisz. Term (a) shows the standard plaquette, which leads to $\mathcal{O}(a^2)$ uncertainty from continuum physical value. Terms (a), (b), and (c) include all a^4 and a^6 terms with different coefficient from (a) and (c). They also include terms at order αa^2, where α is the strong coupling. We can remove the $\mathcal{O}(a^4)$ and $\alpha_s a^2$ terms. We combine (a), (b), and (c) with suitable weight.

Similarly, we can also make improvement on the staggered fermion. In Figure 4.2, we show the terms corresponding to asqtad improvement. For example, the $\mathcal{O}(a^2)$ term is

$$c_1[U_\mu(x)\delta_{y,x+\widehat{x}} - U^\dagger_\mu(x-\widehat{\mu}x)\delta_{y,x-\widehat{\mu}}] \ , \tag{4.28}$$

but with the Naik term:

$$c_3[U_\mu(x)U_\mu(x+\widehat{\mu})U_\mu(x+2\widehat{\mu})\delta_{y,x+3\widehat{\mu}} - \text{ backward term} \tag{4.29}$$

one can get the accuracy up to $\mathcal{O}(a^4)$. This is gained by combination of coefficient c_1 and c_3, which can cancel the a^2 term. One can introduce other terms as illustrated. The result is an action good to order αa^2 and a^2.

4.3 Generation of lattice ensembles

Once we choose a gauge and fermion action (Fermilab for heavy quark and asqtad improved staggered fermion for up and down quark), we will generate the gauge field configurations $U_\mu^{(i)}(x)$, with $i = 1, \cdots, N$. These gauge field configurations are distributed with probability:

$$P(\{U_\mu^{(i)}(x)\}) = \frac{1}{Z_\beta}[\det M_F(U)^{n_f} \exp[-S_G(U)]] \ . \tag{4.30}$$

Then, we can compute average value of the observable O as an average over the ensemble of gauge field configurations:

$$\langle O \rangle = \frac{1}{N}\sum_{i=1}^{N} O^{(i)} \ . \tag{4.31}$$

This is how lattice ensembles of two-point and three-point correlation functions are generated.

4.4 Lattice form factor

To compute the lattice form factor, we need the two-point functions for the B meson and D meson, and a three-point function for the matrix element of the current, shown in Figure 4.3. The process starts with the interpolating operator, which generates a B or D meson from the vacuum plus excited states usally. So we begin with a brief introduction to the interpolating operators. We use:

$$\mathcal{O}_a(x) = \sum_y [\overline{\psi}(y)R(y,x)\Omega(x)]_a\chi(x) \text{ [29]} \ , \tag{4.32}$$

where $\chi(x)$ is the one component field appearing in the staggered action, index a is the lattice spacing, and $\Omega(x) = \gamma_1^{x_1}\gamma_2^{x_2}\gamma_3^{x_3}\gamma_4^{x_4}$ is the transformation connecting naive and staggered fermion.

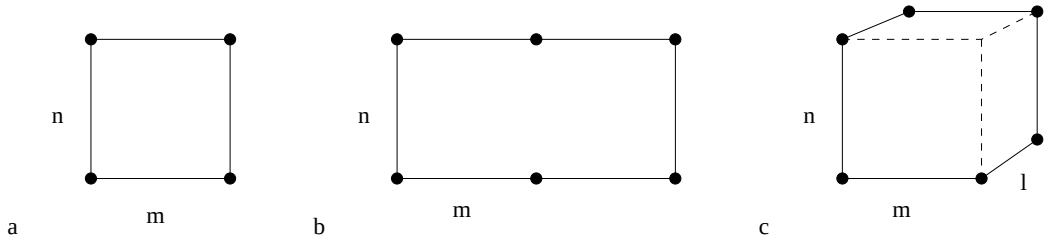

Figure 4.1. Diagrams representing terms in the improvement to the gauge action: (a) standard plaquette, (b) 2×1 rectangle, and (c) $1 \times 1 \times 1$ parallelogram.

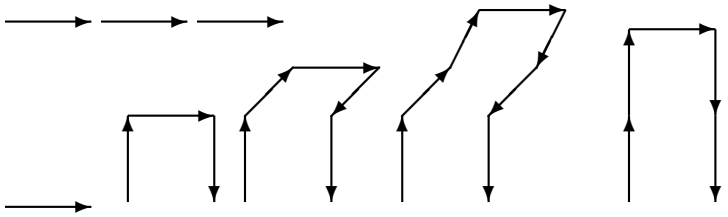

Figure 4.2. Diagrams illustrating the improvement to fermion action (the asqtad improvement). The upper one is the Naik term in asqtad improvement. The lower five terms are the one link term, the Staple term, the five link term, the seven link term, and the Lepage link term, respectively, from left to right.

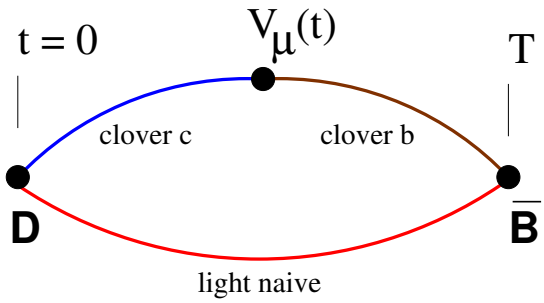

Figure 4.3. Valence quark line diagram for the matrix element of the vector current in the $B \to Dl\nu$ process.

Here, $R(y, x)$ is the smearing function. There are two smearing in the simulation, one is a local (or unsmeared) source $R = \delta_{xy}$, another is a smeared source:

$$R(x, y) = \delta_{x_4 y_4} S(\mathbf{x} - \mathbf{y}) \ . \tag{4.33}$$

For $R(r)$ we take the 1S solution of the Richardson potential for the quarkonium (heavy quark anti-quark $Q\overline{Q}$) systems [30].

With the interpolating operator $\mathcal{O}_{X,a}$, where $X \in B, D$, we can construct the two-point correlation function and expend it in terms the eigenstate of lattice Hamiltonian:

$$C^{2pt,X}(\mathbf{p},T) = \langle \mathcal{O}_X^\dagger(0)\mathcal{O}_X(t)\rangle$$
$$= \sum_n s_n^t Z_n(\mathbf{p})[\exp(-E_n(\mathbf{p})t) + \exp(-E_n(\mathbf{p}))(N_t - t)] \ . \quad (4.34)$$

Here, T is the distance between B meson and D meson at the time dimension. $\mathbf{p}$ is the mass of D meson in the rest frame of B meson. $s_n = \pm 1$ allows for contributions that oscillate/don't oscillate with time. Here, the oscillating terms are generated because a complete specification of the operator spin and parity with staggered formions requires two adjacent time slices, but our inerpolating operator occupies only one. Thus, it contains both parities. One parity contributes a term that oscillates in time. The other contributes a term that does not oscillate. N_t is the lattice extent of t. Z_n is the overlap coefficient of the two-point function. We use both point and 1S smeared interpolating operators for the D meson and 1S smeared interpolating operators for the B meson. With the formula above, we can extract the mass, or energy E_n, and we can also get the overlap factor Z_n. These are building blocks for the form factors.

The three-point function is defined as follows:

$$C^{3pt,X\to Y,\mu}(\mathbf{p};0,t,T) = \langle \mathcal{O}_Y^\dagger(0)V^\mu(t)\mathcal{O}_X(t)\rangle \ , \quad (4.35)$$

where $V^\mu = b\Gamma^\mu c$ is the lattice vector current. The lattice vector current is equal to the continuum vector current in the continuum limit $a \to 0$. However, on the lattice it must be renormalized to give the same result. Here, we define the lattice vector current as V^μ and the continuum vector current as $\mathcal{V}^\mu$. For example, the vector current corresponding to the b to c transition V_{cb}^μ is related to the continuum vector current by the relation $Z_{cb}^\mu V_{cb}^\mu = \mathcal{V}_{cb}^\mu$. The diagonal factors Z_{cc}^μ and Z_{bb}^μ are nonperturbatively determined, but Z_{cb}^μ is not easily calculated. So we treat it approximately in the following way:

$$Z_{cb}^\mu = \rho_{cb}^\mu \sqrt{Z_{cc}^\mu Z_{bb}^\mu} \ . \quad (4.36)$$

Then, ρ_{cb}^μ is determined approximately from the one-loop lattice perturbation theory. We will do the renormalization according to this relation to get a more accurate value for the continuum form factor. For example, we have the following relation:

$$h_{+,cont.}(w) = \rho_{cb}^4 h_{+,lat.}(w)$$
$$h_{-,cont.}(w) = \rho_{cb}^1 h_{-,lat.}(w) \ . \quad (4.37)$$

Here, ρ_{cb}^4 is already available, but ρ_{cb}^1 is still not available since it is a complicated calculation. We will describe how we deal with this quantity in the next chapter. In the ρ factor, we

introduced a blinding factor, which will finally be provided by people in our collaboration to get the final value of $|V_{cb}|$. We introduce it to avoid the bias on the determination of this CKM matrix element. We use these considerations, carefully illustrated in Chapter 5.

Both two-point and three- point function are used in our analysis. These form factors are constructed from naive light spectator quark (the up or down quark in B and D meson which don't take part in the weak interaction) propagators and clover heavy quark propagators in the Fermilab interpretation. Valence (the quarks determine the total charge of meson) bottom and charm quark masses were tuned to the kinematic B_s and D_s masses. The mass of the asqtad light spectator quark is set equal to that of the light sea quark.

So once we get the three-point function such as $\langle D(\mathbf{p})|V^4|B(\mathbf{0})\rangle$, we can construct the following form factors to get the vector current using parameterization with h_+ and h_-:

$$\begin{aligned} R_+(\mathbf{p}) &\equiv \langle D(\mathbf{p})|V^4|B(\mathbf{0})\rangle \\ R_-(\mathbf{p}) &\equiv \frac{\langle D(\mathbf{p})|V^1|B(\mathbf{0})\rangle}{\langle D(\mathbf{p})|V^4|B(\mathbf{0})\rangle} \\ x_f(\mathbf{p}) &\equiv \frac{\langle D(\mathbf{p})|V^1|D(\mathbf{0})\rangle}{\langle B(\mathbf{p})|V^4|B(\mathbf{0})\rangle} \\ w(\mathbf{p}) &\equiv [1+x_f(\mathbf{p})^2]/[1-x_f(\mathbf{p})^2] \end{aligned} \tag{4.38}$$

$$\begin{aligned} h_+(\mathbf{p}) &\equiv R_+(\mathbf{p})[1-R_-(\mathbf{p})x_f(\mathbf{p})] \\ h_-(\mathbf{p}) &\equiv R_+(\mathbf{p})[1-R_-(\mathbf{p})/x_f(\mathbf{p})]\ . \end{aligned} \tag{4.39}$$

Here, for zero recoil, previous work [6] used the double ratio defined as follows to suppress the statistical error:

$$R_+(1) = \rho_{cb}^4 \frac{\langle D|\bar{c}\gamma^0 b|B\rangle\langle B|\bar{b}\gamma^0 c|D\rangle}{\langle D|\bar{c}\gamma^0 c|D\rangle\langle B|\bar{b}\gamma^0 b|B\rangle} \equiv |h_+(1)|^2\ . \tag{4.40}$$

We take the square root of this value to extract $h_+(w)$. We will use a similar method to reduce the error in the nonzero recoil form factor. We will also discuss these in detail in the next chapter.

CHAPTER 5

ANALYSIS OF DATA

For this chapter, we discuss how to calculate the form factor and get a precise value of $|V_{cb}|$. We started from two-point and three-point correlators calculated on fourteen ensembles by the Fermilab-MILC collaboration with lattice spacing as small as 0.045 fm and light-to-strange-sea-quark mass ratios as low as 1/20. These lattice ensembles are summarized in Figure 5.1. As shown in the figure, these 14 ensembles are with different lattice spacing and different quark masses. We call those ensembles with lattice spacing approximately 0.12 fm *coarse* ensembles, the ones with lattice spacing about 0.09 fm *fine* ensembles, the ones with lattice spacing about 0.06 fm *superfine* ensembles, and finally the one with 0.045 fm *ultrafine* ensemble. For each lattice spacing, we have ensembles with different light quark mass, but the strange quark mass close to the physical value. Since it is very expensive to simulate with physical up and down quark masses, we are using large unphysical quark masses. In this figure, we are using physical strange quark mass as a scale to denote the magnitude of light quark mass, namely using $m_{u,d}/m_s$. In this simulation, the light valence quark mass is set to be the same as the sea quark mass. We use these many ensembles with different lattice spacing and light quark mass to carry out extrapolation to zero lattice spacing and physical light quark mass. The analysis proceeds as follows: (1) Calculate the two point and three point functions, on each of these 14 ensembles. (2) Fit to extract the energies and overlap factors of the B and D mesons from the jackknife samples of two-point function. (3) Construct the form factors from two-point and three-point functions. (4) Since we are measuring form factors at nonzero lattice spacing, and unphysical m_l, and what we want is the continuum value of the form factor at physical m_l so that we can compare with experiment, we extrapolate in quark mass m_l and lattice spacing to get the physical value of form factor. (5) Finally, we fit our result together with the experimental result to get $|V_{cb}|$.

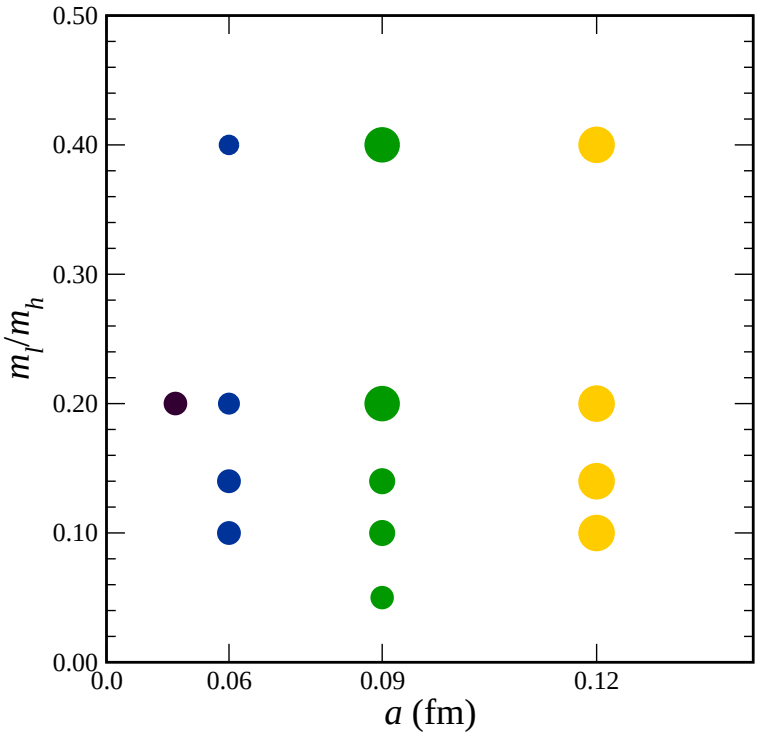

Figure 5.1. (color online) Each disk represents one ensemble. The plot coordinates show range of lattice spacings and light-quark masses used here (colored or gray discs). In our notation, $m_l = m_{u,d}$ is the average mass of up and down quark and $m_h = m_s$ is the mass of the strange quark. The area is proportional to the size of the ensemble. The size varies from 600 to 2000 configuration files. The physical mass ratio is $m_l/m_s = 1/27 \approx 0.04$.

5.1 Two-point correlation function

As introduced in section 4.4, in lattice QCD simulation, we make use of smeared or local interpolating operators $\mathcal{O}_{X,a}$ with $X \in B, D$, to calculate the hadronic correlation function. To analyze the two point correlation function, we use the following equation:

$$C^{2pt,X}(\mathbf{p}, t) = \sum_n s_n^t Z_n(\mathbf{P})[\exp(-E_n(\mathbf{p}t)) + \exp(-E_n(\mathbf{p}))(N_t - t)] \ . \tag{5.1}$$

Here, $s_n = (-)^t$ or 1 gives the contribution that either oscillates in time or not. As discussed in section 4.4, N_t is the lattice extent in t. Z_n is the overlap coefficient of the interpolating operator. We use both point and 1S smeared interpolating operators for the D meson and 1S smeared interpolating operators for the B meson. Fitting the lattice measurements to the formula above, we can extract the mass, or energies E_n, and we can also get the overlap factors Z_n.

When we fit the measured correlation function to Equation (5.1), we keep only the first few terms. The other terms fall off more rapidly with large t. Truncating the series risks

distorting the values of the terms we keep. We usually keep the same number of oscillating and nonoscillating terms, so we count them in pairs. The first pair is the ground state in both cases, the second is the first excited state, etc.. So we try different numbers of pairs and we vary the fit range $[t_{min}, t_{max}]$. We look for a good chi square and stability of the result against increases in t_{min} and number of pairs kept. We list the result of both energy and overlap function, and compare the central value, error, and the confidence level. We use $2+2$ and $3+3$ to denote different numbers of pairs. By $2+2$, we mean two pairs of energies, ground and first excited state mass, together with their oscillating partners. By $3+3$, we are adding the second excited state and its oscillating partner. The result of the ground state mass and overlap function for the 0.12 fm (coarse) ensemble are collected in Table 5.1 and Table 5.2, respectively.

We choose different $[t_{min}, t_{max}]$ because there is more excited state contamination at regions where t is close to 0. As shown in Figure 5.2, with $t_{min} = 3$ for $3+3$ fit, we get a result statistically consistent with the $2+2$ fit, where we use $t_{min} = 6$. The size of the circle shows the goodness of the fit on each data point. The larger the circle, the better the fit. So for the 0.12 fm (coarse) ensemble, we settled on $[3, 23]$ as the ideal choice. We use the same scheme to choose fitting ranges of other ensembles.

5.2 Three-point correlation function

With the above approach to analyze two-point function, we obtain energies of the ground state and excited states and overlap factors. They will be used to analyze the three-point functions. For illustration, we show the reduction of the three-point function to obtain $R_+(p) = \langle D(\mathbf{p})|V^4|B(\mathbf{0})\rangle$. In our analysis, we include excited B and D contributions indicated with a prime but not both together, since it is expected to be small:

$$\begin{aligned} C_{V4}^{3pt,B\to D}(\mathbf{p},t) &= \sqrt{Z_D(\mathbf{p})}\frac{e^{-E_D t}}{\sqrt{2E_D}}\left\langle D(\mathbf{p})|V^4|B(\mathbf{0})\right\rangle \frac{e^{-m_B(T-t)}}{\sqrt{2m_B}}\sqrt{Z_B(\mathbf{0})} \\ &+ \sqrt{Z_{D'}(\mathbf{p})}\frac{e^{-E_{D'} t}}{\sqrt{2E_{D'}}}\left\langle D'(\mathbf{p})|V^4|B(\mathbf{0})\right\rangle \frac{e^{-m_B(T-t)}}{\sqrt{2m_B}}\sqrt{Z_B(\mathbf{0})} \\ &+ \sqrt{Z_D(\mathbf{p})}\frac{e^{-E_D t}}{\sqrt{2E_D}}\left\langle D(\mathbf{p})|V^4|B'(\mathbf{p})\right\rangle \frac{e^{-m_{B'}(T-t)}}{\sqrt{2m_{B'}}}\sqrt{Z_{B'}(\mathbf{0})}\,, \end{aligned} \tag{5.2}$$

or

$$\begin{aligned} C_{V^4}^{3pt,B\to D}(\mathbf{p},t) &= C_0(\mathbf{p})\left\langle D(\mathbf{p})|V^4|B(\mathbf{0})\right\rangle e^{-E_D t}e^{-m_B(T-t)} \\ &\quad \left[1 + C_1(\mathbf{p})e^{-\Delta E_D t} + C_2(\mathbf{p})e^{(t-T)\Delta m_B}\right], \end{aligned} \tag{5.3}$$

where $C_0(\mathbf{p})$, $\Delta E_D = E_{D'} - E_D$, and $\Delta m_B = m_{B'} - m_B$ come from fits to two-point correlators. Terms oscillating as $(-)^t$ (not shown) appear in the three-point function just

Table 5.1. Comparison of ground state for $2+2$ and $3+3$ two-point fits for the D meson on the 0.14 m_s 0.12 fm (coarse) ensemble.

p	$2+2$ E_D	$3+3$ E_D	2+2 range	3+3 range	2+2 χ./d.o.f	3+3 χ./d.o.f.
000	0.9567(7)	0.9566(7)	[6, 16]	[3, 23]	18.9/18	36.4/40
110	1.0445(11)	1.0433(12)	[6, 16]	[3, 23]	16.5/18	33.8/40
111	1.0849(16)	1.0831(15)	[6, 16]	[3, 23]	22.6/18	39.3/40
200	1.1199(23)	1.1172(23)	[6, 16]	[3, 23]	17.4/18	38/8/40

Table 5.2. Comparison of overlap factors of different two-point fits of 0.14 m_s 0.12 fm (coarse) ensemble.

p	2+2 $Z_{1S,1S}$	3+3 $Z_{1S,1S}$	2+2 $Z_{d,d}$	3+3 $Z_{d,d}$
000	4.046(31)	4.049(34)	0.0789(7)	0.0785(8)
100	2.936(24)	2.907(33)	0.0751(8)	0.0738(9)
110	2.185(25)	2.147(32)	0.0715(9)	0.0699(11)
111	1.662(27)	1.618(31)	0.0685(13)	0.0663(13)
200	1.285(31)	1.235(35)	0.0658(19)	0.0629(19)

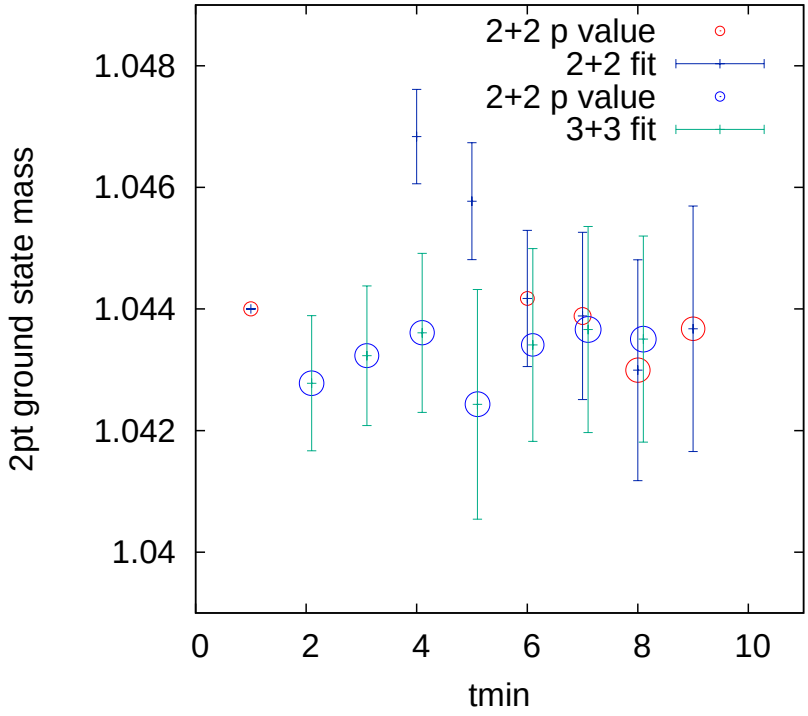

Figure 5.2. Plot of ground state energy in lattice units vs the minimum time $t = t_{min}$. This plot is done with momentum 110. The point at $t = 1$ is the sample point with p value 0.5. The size of the circle represent the magnitude of the p value.

as in the two-point. Our objective is to determine the form factors and ratio of form factors in Equation (4.39). Because there are excited state contributions, it is necessary to fit the three-point functions as a function of t and extract the ground state term. So R_+, R_-, and x_f in Equation (4.39) each have time-dependent version. For example, the form factors, like $R_+(t, T; \mathbf{p})$ are defined in the following way:

$$R_+(t,T;\mathbf{p}) = \frac{C_{V_4}^{3pt,B\to D(t,T;\mathbf{p})}}{\sqrt{C_{V_4}^{3pt,D\to D}(t,T;\mathbf{0})C_{V_4}^{3pt,B\to B}(t,T;\mathbf{0})}} \frac{Z_D(\mathbf{0})E_D}{Z_D(\mathbf{p})m_D} e^{E_D t - \frac{1}{2}m_D T} e^{-m_B(t-\frac{1}{2}T)} \quad (5.4)$$

and $R_+(\vec{p})$ is term in the fit that is constant in t. We suppress their contributions by averaging over T, $T+1$ and t, $t+1$, as introduced in [31]. The average equation is as follows:

$$\begin{aligned} C_{avg}^{X\to Y}(0,t,T) \equiv & \frac{1}{2}C^{X\to Y}(0,t,T) + \frac{1}{4}C^{X\to Y}(0,t,T+1) \\ & + \frac{1}{4}C^{X\to Y}(0,t+1,T+1)\ . \end{aligned} \quad (5.5)$$

The zero recoil form factor $R_+(0,t)$ can be obtained in two ways, Equation (5.4) or using the double ratio in Equation (4.40). The latter is more precise because fluctuations cancel

in the ratio. Likewise fluctuations tend to cancel in the ratio $R_+(\overrightarrow{p},t)/R_+(0,t)$, based on Equation (5.4). So we compute this ratio for nonzero recoil and then multiply by $R_+(0,t)$ computed from the double ratio.

So at nonzero recoil, we start by fitting the ratio to the following expected form that includes the ground state and first excited state contributions:

$$\frac{R_+(\mathbf{p},t)}{R_+(\mathbf{0},t)} = \frac{R_+(\mathbf{p})}{R_+(\mathbf{0})}\exp(\delta m\, t) + A(\mathbf{p})\exp(-\Delta E_D t) + B(\mathbf{p})\exp(\Delta m_B t)\,, \tag{5.6}$$

where we expect $\delta m = 0$, $\Delta E_D = E_{D'} - E_D$, and $\Delta m_B = m_{B'} - m_B$, *i.e.,* values from the two-point functions. Since the three-point functions contain new information about δm, ΔE_D, and Δm_B we introduce Bayesian priors to constrain these parameters when fitting to Equation (5.6). The central values and widths of priors come from fits to the two-point functions.

The result of the fit is value of $R_+(p)/R_+(0)$. We do a similar fit for $R_-(\overrightarrow{p})$ and $x_f(\overrightarrow{p})$. Once we get R_+, R_- and x_f, we construct h_+ and h_- for all the ensembles.

5.3 Heavy-quark mass correction

The simulation values of the heavy quark mass parameters κ_c and κ_b were not our final, best tuned values. Updated kappa value were obtained from a more precise determination of quark mass. So we need to adjust the form factor we get in the previous section according to the change of kappa value. The change is small. So we make the adjustment by computing the first-order correction in a Taylor series in $1/m_c$ and $1/m_b$. For this, we computed the first derivatives of the form factors in a special numerical simulation done at multiple heavy quark masses, and then took the numerical derivative. For the mass depenence $1/m_c$ and $1/m_b$, we use the tree-level tadpole-corrected kinematic mass, defined in terms of the bare mass m_b as follows:

$$\begin{aligned} m_0 a &= \frac{1}{(2u_0)}\cdot\left(\frac{1}{\kappa} - \frac{1}{\kappa_{cr}}\right) \\ \overline{m_1 a} &= \log(1 + m_0 a) \\ \overline{m_2 a}^{-1} &= \frac{2}{m_0 a\cdot(2 + m_0 a)} + \frac{1}{m_0 a + 1}\ . \end{aligned} \tag{5.7}$$

Here, u_0 is the tadpole parameter, which is taken from the average plaquette for the gluon and sea-quark action. m_0 is tadpole-improved bare quark mass for SW quarks. m_1 and m_2 are rest mass and kinetic mass, respectively, from the dispersion relation. Up to first-order

in the inverse quark masses in heavy quark effective theory, the form factor h_+ depends on the charm and bottom quark masses through

$$h_+(w) = \xi(w) + (\frac{1}{m_c} + \frac{1}{m_b})L_1(w) \ , \tag{5.8}$$

where $\xi(w)$, the Isgur-Wise function, satisfies $\xi(1) = 1$ and the coefficient of the first-order correction satisfies Luke's theorem, namely $L_1(1) = 0$. In our chiral/continuum fit model, we parameterized h_+ as follows:

$$h_+(a, m_l, w) = 1 - \rho_+^2(w-1) + k_+(w-1)^2 \ldots . \tag{5.9}$$

For purposes of doing the kappa adjustment, we use a linear approximation for both $\xi(w)$ and $L_1(w)$, leading to

$$h_+(a, m_l, w) = 1 - \rho_{+,\text{eff}}^2(w-1) \, , \tag{5.10}$$

where the slope depends on the quark masses. A fit to $h_+(w)$ for the 0.12 fm 0.2 m_s ensemble gives $\rho_{+,\text{eff}}^2 = 1.21(6)$ with $p = 0.44$. In the following, we drop the "eff" label on ρ_+^2.

We measure the form factor at discrete values of the recoil momentum of the D meson. This leads to discrete values w_i. When we shift the mass of the charm quark, w_i changes. However, it does not change when we shift the mass of the bottom quark. We take the convention that when we shift both quark masses, we shift w_i to w_i' and we shift $h(w_i)$ to $h'(w_i')$.

We define two shifts, one, a partial shift of h_+ at constant w_i

$$dh_{+i} = h'_+(w_i) - h_+(w_i) \ , \tag{5.11}$$

and one, the full shift of both h_+ and w_i:

$$dh'_{+i} = h'_+(w_i') - h_+(w_i) \ . \tag{5.12}$$

The partial shift is

$$dh_+(w) = -d\rho_+^2(w-1) \, , \tag{5.13}$$

and the full shift is

$$dh'_+(w_i) = h'_+(w_i') - h'_+(w_i) + h'_+(w_i) - h_+(w_i) = -\rho_+^2 dw_i + dh_+(w_i) \, . \tag{5.14}$$

We also model the shift in w_i with a linear expression:

$$dw(w) = d\rho_w(w-1) \ , \tag{5.15}$$

so we have, finally

$$dh'_+(w) = (-\rho_+^2 d\rho_w - d\rho_+^2)(w-1)\,. \tag{5.16}$$

For the specific shift from $h_+(w_i)$ at $\kappa_c = 0.1254$ to $h'_+(w'_i)$ at $\kappa_c = 0.1280$ we have ($p = 0.34$)

$$dh_+(w) = dh'_+(w) + \rho_+^2 d\rho_w(w-1) = -d\rho_+^2(w-1) \tag{5.17}$$

The fit gives $d\rho_+^2 = -0.056(12)$. We also have ($p = 0.61$)

$$dw(w) = d\rho_w(w-1)\ . \tag{5.18}$$

Heavy quark effective theory suggests generalizing the shift by considering derivatives with respect to $1/m_{2c}$, the inverse kinetic charm-quark mass. The shift in κ_c implies

$$dh_+(w_i) = d\rho_w(w_i-1)\ , \tag{5.19}$$

or, generalizing,

$$dh_+(w_i) = (r_{\rho_+,b}(w_i-1))dm_{2b}^{-1}\ . \tag{5.20}$$

Here, $r_{\rho,b} = 0.35(23)$.

We are now in a position to check the prediction of heavy quark effective theory in Equation (5.8), namely that at fixed w, the derivatives with respect to $1/m_{2c}$ and $1/m_{2b}$ are equal. To make this comparison, we see that $r_{\rho_+;c} \simeq r_{\rho_+;b}$.

With the formula above, we are able to predict

$$dh_+(\text{total}) = dh_+(\text{charm}) + dh_+(\text{bottom})\ .$$

With the table of dm_2^{-1} for a different ensemble, as we show in Table 5.3, we can get all of the corresponding shifts of h_+ and w on each ensemble, and on each jackknife sample. Because the ratio $r_{\rho_+,c}$ of charm quarks has better statistics, we use its value for the bottom quark kappa-tuning correction.

Making use of the same ensembles $(\kappa_c, \kappa_b) = (0.1254, 0.0901)$ and $(\kappa_c, \kappa_b) = (0.1280, 0.0901)$, we conduct kappa tuning correction for h_-.

Again, in our chiral/continuum fit model, we parameterized h_- as follow:

$$h_-(a, m_l, w) = c_1 - \rho_-^2(w-1) + k_-(w-1)^2 \cdot \cdot \tag{5.21}$$

In order to do the kappa adjustment, we use a linear approximation, which leads to the following relation:

Table 5.3. Kappa tuning correction in lattice units. To use these numbers for the kappa tuning correction, we use the r_1/a value provided by [3].

β	m_l/m_h	$dM_2^{-1}(charm)$	$dM_2^{-1}(bottom)$
6.76	0.1	-0.16695	-0.04963
6.76	0.14	-0.16695	-0.04963
6.76	0.2	-0.16762	-0.04966
6.79	0.4	-0.2118	-0.062295
7.075	0.05	-0.10115	-0.02725
7.08	0.1	-0.0915	-0.025
7.085	0.14	-0.081485	-0.025205
7.09	0.2	-0.098919	-0.0277043
7.11	0.4	-0.0886674	-0.023584
7.46	0.1	-0.0263945	-0.0073766
7.465	0.14	-0.015891	-0.0036975
7.47	0.2	0	0
7.48	0.4	-0.063039	-0.022108
7.81	0.2	-0.083177	-0.181127

$$h_-(a, m_l, w) = c_1 - \rho^2_{-,eff}(w-1) \ , \tag{5.22}$$

where the slope depends on the quark mass. A fit to $h_-(w)$ for the 0.12 fm 0.2 m_s ensemble gives $\rho^2_{-,eff} = -0.19(5)$ with $p = 0.019$.

The analysis of the shift in h_- is similar to h_+. The full shift is:

$$dh'_-(w_i) = -\rho^2_- dw_i + dh_-(w_i) \ . \tag{5.23}$$

Using the same expression for $dw(w)$, we have, finally:

$$dh'_-(w) = dc_1 + (-\rho^2_- d\rho_w - d\rho^2_-)(w-1) \ . \tag{5.24}$$

For the specific shift from $h_-(w_i)$ at $\kappa_c = 0.1254$ to $h'_-((w'_i)$ at $\kappa_c = 0.1280$, we have $(p = 0.85)$.

Then, we get the formula for h_- as follow:

$$dh_-(w) = dh'_-(w) - \rho_- dw(w) \ . \tag{5.25}$$

Dividing by the inverse charm mass, we get the following formula for dh_-:

$$dh_- = (c_0 + c_1(w_i - 1))dm_{2b^{-1}} \ . \tag{5.26}$$

where c_0 and c_1 are coefficients which we get from different fits we mentioned here.

For the bottom quark, there is no shift in w_i. For the shift in κ_b from 0.0901 to 0.0860, we fit $(p = 0.91)$:

$$dh_- = dc_1 - d\rho^2_{-,b}(w_i - 1) \ , \tag{5.27}$$

giving:

$$dh_- = -0.0108(6) + 0.018(8)(w_i - 1) \ , \tag{5.28}$$

or:

$$dh_- = (0.48(2) - 0.83(35)(w_i - 1)dm_b^{-1} \ . \tag{5.29}$$

As an example, in Table 5.4, we show the kappa tuning correction for the coarse 0.14 m_s for both h_+ and h_-. As we see, the corrections in this worst case ensemble are smaller than the statistical in nearly all cases.

Table 5.4. Comparison for old and new value of w, h_+, and h_- for the 0.14 m_s 0.12 fm ensemble.

momentum	old w	new w	old h_+	new h_+	old h_-	new h_-
000	1	1	1.0156(42)	1.0156(42)	NA	NA
100	1.04613	1.04608	0.9652(54)	0.9647(54)	-0.1177(66)	-0.1190(66)
110	1.08885	1.08875	0.9175(64)	0.9165(64)	-0.1094(79)	-0.1108(79)
111	1.12778	1.12764	0.8802(87)	0.8786(87)	-0.1025(100)	-0.1040(101)
200	1.15866	1.15848	0.8582(107)	0.8563(107)	-0.0778(122)	-0.0793(124)

5.4 Chiral-continuum extrapolation

The construction of the form factor requires information from both two-point and three-point functions on each ensemble. These functions are determined from the same gauge configurations, so the values are corrected. Those correlations carry through the correlations in h_+ and h_-. Results from different ensembles are uncorrelated. We use the single-elimination jackknife method to take account of these correlations. By single elimination jackknife, we mean we reconstruct samples which exclude one of the configuration. We carry through all fits to two-point and three-point functions on each sample—several hundred cases in each ensemble. So for each jackknife sample on each ensemble, we get values of h_+ and h_- as a function of w, from which we determine the covariance matrix for the values of h_+ and h_-—*i.e.,* the standard deviations correlations between form factors with different momenta within the same ensemble. Then, since data in different ensembles are statistically independent, we can build up a block diagonal covariance matrix for all the ensembles put together. With this information, we can then fit h_+ and h_- simultaneously. Before fitting, we do the kappa tuning adjustment according to the previous section.

The resulting form factors h_+ and h_- are shown in Figure 5.3. We fit them to the expressions

$$\begin{aligned} h_+(a,m_\ell,w) &= 1-\rho_+^2(w-1)+k_+(w-1)^2+\frac{X_+(\Lambda_\chi)}{m_c^2} \\ &\quad +c_{1,+}m_\ell+c_{a,+}a^2+c_{a,w,+}a^2(w-1) \\ &\quad +\frac{g^2_{D^*D\pi}}{16\pi^2 f^2}\mathrm{logs}_{1-\mathrm{loop}}(\Lambda_\chi,w,m_\ell,a) \qquad (5.30) \\ h_-(a,m_\ell,w) &= \frac{X_-}{m_c}-\rho_-^2(w-1)+k_-(w-1)^2+c_{1,-}m_\ell+c_{a,-}a^2+c_{a,w,-}a^2(w-1)\ . \end{aligned}$$

Here, $\rho^2_\pm$ is the coefficient of the linear term of $w-1$ for $h_\pm$, $k_\pm$ is the coefficient of the curvature term $(w-1)^2$. The $X_\pm$ term uses notation from heavy quark effective theory which gives a correction to the leading terms.

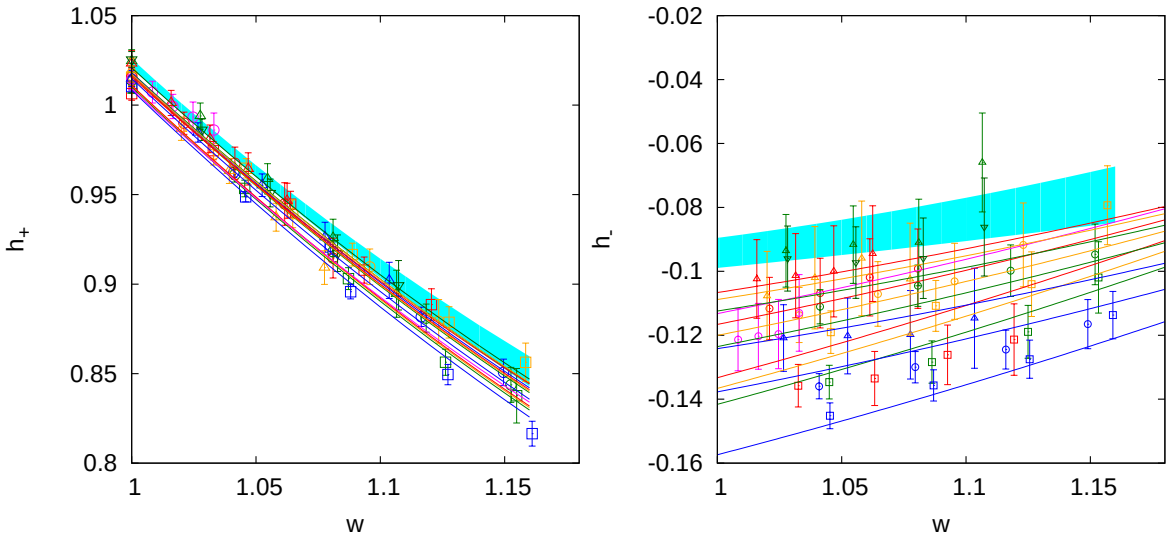

Figure 5.3. Global fit of all data for the form factors h_+ (the left) and h_- (the right) vs w, the recoil parameter w. The simultaneous fit gives $p = 0.27$. Blue band gives the physical continuum prediction. Rainbow color spectrum encodes $m_l = m_s$: blue to red for large to small. Symbol shapes encode lattice spacing: square, circle, triangle for coarser to finer.

Other parameters are the light spectator quark mass m_ℓ, the lattice spacing a, and the recoil parameter $w = v \cdot v'$. For the one-loop chiral logs, we use a staggered fermion version of the formula in the paper of Chow and Wise [20]. Thus, these fit functions contain the correct next-to-leading-order chiral perturbation theory expressions, including staggered discretization effects [21]. As can be seen, the dependence of h_+ on a and m_ℓ/m_h is quite mild. However, h_- shows a stronger dependence on them. From HQET, we expect h_- to have larger discretization effects than h_+, because h_- has first-order terms in $1/am_c$ and $1/am_b$ over the entire w range, whereas in h_+, those terms are suppressed at small w. $|V_{cb}|$, the contribution coming from h_- over the entire kinematic range is small, so the larger errors in h_- do not affect the overall error much. These features with 14 ensembles are consistent with our previous findings with four ensembles [21]. The central values and statistical errors of the fit parameters in the h_+ and h_- data are collected in Table 5.5. The correlation matrix is as summarized in Table 5.6. With this information, we can then predict the extrapolated values of f_+ and f_0 at the physical quark mass and zero lattice spacing. We call the predicted values *synthetic data*.

5.4.1 Construction of synthetic data of f_+ and f_0

For the final step in the analysis, we need predicted values of f_+ and f_0 at selected values of w, their errors, and their covariance. We call this our *synthetic data*. This subsection

Table 5.5. Best parameter values and errors from a combined chiral/continuum fit of h_+ and h_-. Parameters are used in Equation (5.30). Correlation coefficients are given in Table 5.6.

coefficient	**result**	
$1 + X_+/m_c^2$	c_0	1.031(4)
m_l	c_1	−0.16(6)
$-\rho_+^2$	c_2	−1.16(6)
a^2	c_3	0.11(3)
k_+	c_4	1.11(16)
$g_{D^*D\pi}/(16\pi^2 f^2)$	c_5	0.26(8)
$a^2(w-1)$	c_6	−0.3(5)
X_-	d_0	−0.092(5)
m_l	d_1	−0.55(9)
$-\rho_-^2$	d_2	0.11(4)
a^2	d_3	−0.19(5)
k_-	d_4	0.14(16)
$a^2(w-1)$	d_5	0.7(4)

explains how we get the central values and covariance. The vector space of coefficients of the fit parameters for h_+ has 7 elements in Equation (5.30), while h_- has 6 elements. To get f_+ and f_0, we need a linear combination of the resulting vector with 13 components. The linear combination comes from Equation (3.16). We use the following notation:

$$\begin{aligned} a_i &= c_i \qquad i = 0, \cdots, 6 \\ a_i &= d_{i-7}, i = 7, \cdots, 12 \ , \end{aligned} \tag{5.31}$$

and we get the linear combination for the synthetic data at selected w_j.

$$\begin{aligned} f_+(w_j) &= \sum_{i=0}^{12} a_i g_{+,i}(w_j) \\ f_0(w_j) &= \sum_{i=0}^{12} a_i g_{0,i}(w_j) \ . \end{aligned} \tag{5.32}$$

We have defined:

$$\begin{aligned} g_+(w,a,m) &= \{e_1, e_1 m, e_1(w-1), e_1 a^3, e_1(w-1)^2, e_1 0.1497895 Log(w), \\ &\quad e_1 a^2(w-1), e_2, e_2 m, e_2(w-1), e_2 a^2, e_2(w-1^2), e_2 a^2(w-1))\} \\ g_0(w,a,m) &= \{q_1, q_1 m, q_1(w-1), q_1 a^3, q_1(w-1^2), q_1 0.1497895 Log(w), q_1 a^2(w-1) \\ &\quad , q_2, q_2 m, q_2(w-1), q_2 a^2, q_2(w-1)^2, q_2 a^2(w-1)\} \ , \end{aligned} \tag{5.33}$$

Table 5.6. Correlation matrix of coefficients for h_+ and h_-.

	c_0	c_1	c_2	c_3	c_4	c_5	c_6	d_0	d_1	d_2	d_3	d_4	d_5
c_0	1.000	−0.631	0.099	−0.678	−0.026	0.643	0.262	−0.130	0.068	−0.060	0.094	−0.007	0.060
c_1	−0.631	1.000	−0.170	−0.053	0.016	−0.428	−0.054	0.063	−0.141	0.002	0.024	0.013	−0.006
c_2	0.099	−0.170	1.000	0.086	−0.322	0.413	−0.714	-0.006	−0.023	0.037	−0.000	0.046	−0.051
c_3	−0.678	−0.053	0.086	1.000	0.010	−0.294	−0.305	0.124	0.019	0.079	−0.166	−0.018	−0.080
c_4	−0.026	0.016	-0.322	0.010	1.000	−0.083	−0.073	−0.017	−0.003	0.004	0.039	−0.066	0.022
c_5	0.643	−0.428	0.413	−0.294	−0.083	1.000	0.144	0.007	−0.001	0.005	−0.007	−0.010	−0.002
c_6	0.262	−0.054	−0.714	−0.305	−0.073	0.144	1.000	−0.003	0.033	−0.052	−0.000	0.036	0.045
d_0	−0.130	0.063	−0.006	0.124	−0.017	0.007	−0.003	1.000	−0.448	0.447	-0.777	−0.062	−0.424
d_1	0.068	-0.141	-0.023	0.019	-0.003	−0.001	0.033	−0.448	1.000	−0.050	−0.108	0.063	0.044
d_2	−0.060	0.002	0.037	0.079	0.004	0.005	−0.052	0.447	−0.050	1.000	−0.433	−0.195	−0.892
d_3	0.094	0.024	−0.000	−0.166	0.039	−0.007	−0.000	−0.777	−0.108	−0.433	1.000	0.010	0.490
d_4	-0.007	0.013	0.046	−0.018	−0.066	-0.010	0.036	−0.062	0.063	−0.195	0.010	1.000	−0.082
d_5	0.060	−0.006	−0.051	−0.080	0.022	−0.002	0.045	−0.424	0.044	−0.892	0.490	−0.082	1.000

and

$$\begin{aligned} e_1 &= \frac{1}{2\sqrt{r}}(1+r) \\ e_2 &= -\frac{1}{2\sqrt{r}}(1-r) \\ q_1(w) &= \sqrt{r}\frac{w+1}{1+r} \\ q_2(w) &= -\sqrt{r}\frac{w-1}{1-r}\ , \end{aligned} \tag{5.34}$$

For the continuum extrapolation, we set $a = 0$, and also $m = m_l$.

We want the covariance $\langle \delta f_{+,0}(w_j)\delta f_{+,0}(w_e)\rangle$. The covariance matrix $\langle \delta a_i \delta a_k\rangle$ is related to it by a linear transformation. Here, $\delta a_i = a_i - \overline{a}_i$, where $\overline{a}_i$ is the best fit value, a_i is the fit value fluctuating around best fit value. The linear relation is written as follows:

$$\langle \delta f_{+,0}(w_j)\delta f_{+,0}(w_l)\rangle = \sum_{ik} g_{+,0,i}(w_j)\langle \delta a_i \delta a_k\rangle g_{+,0,k}(w_l)\ . \tag{5.35}$$

Here, $f_{+,0}$ denotes form factor f_+ or f_0 and $\delta f_{+,0} = f_{+,0} - \overline{f}_{+,0}$.

5.5 z expansion

After we do the chiral/continuum fit and get physical continuum values for the form factors, f_+ and f_0 and their covariance, we fit with fitting model to extrapolate/interpolate them in w and compare them with the experiment result. There are a number of models to choose from, but the z expansion method offers a relatively model independent parameterization that takes account of unitarity and the known analytic structure of the form factor.

We use the z-expansion of Boyd, Grinstein, and Lebed [32], which provides a model-independent parameterization of the q^2 dependence of f_+ and f_0. This expansion builds in constraints from analyticity and unitarity. It is based on the conformal map

$$z(w) = \frac{\sqrt{1+w} - \sqrt{2}}{\sqrt{1+w} + \sqrt{2}}\,, \tag{5.36}$$

which maps the physical region $w \in [1, 1.59]$ to $z \in [0, 0.0644]$. It pushes poles and branch cuts far away to $|z| \approx 1$. Form factors are then parameterized as

$$f_i(z) = \frac{1}{P_i(z)\phi_i(z)} \sum_{n=0}^{\infty} a_{i,n} z^n \,, \tag{5.37}$$

where $P_i(z)$ are the *Blaschke factors* where zero encodes poles in z and ϕ_i are the *outer functions* that remove phase space factors and lead to a simple unitarity bound,

$$\sum_n |a_{i,n}|^2 \leq 1 \,. \tag{5.38}$$

In this work, we do not introduce any pole, so $P_i(z) = 1$. For f_+ and f_0, the outer functions are:

$$\begin{aligned} \phi_+(z) &= \Phi_+(1+z)^2(1-z)^{1/2}[(1+r)(1-z)+2\sqrt{r}(1+z)]^{-5} \\ \phi_0(z) &= \Phi_0(1+z)(1-z)^{3/2}[(1+r)(1-z)+2\sqrt{r}(1+z)]^{-4} \,. \end{aligned} \tag{5.39}$$

Here, $\Phi_0 = 0.5299$, $\Phi_+ = 1.1213$.

In practice, we need only the first few coefficients in the expansion.

To implement the z expansion, we start from the value of f_+ and f_0 at the physical point, as determined from the chiral/continuum fit. We choose three z values, namely $w = 1, 1.08$, and 1.16, and use the corresponding form factor values to determine the coefficients $a_{i,0}$, $a_{i,1}$, $a_{i,2}$, and $a_{i,3}$. The reason for choosing only these six data points is that we only have a few parameters left in the fitting model when we go to the continuum limit, namely $a = 0$ and $m = m_{phys}$. These, then, are used to parameterize the form factors over the full kinematic range, as shown in section 5.7. In the fit, we introduce a Bayesian prior for $a_{i,3}$, because we only have a total of 6 data points, but 8 parameters. We base the prior in the unitarity bound 5.38, use a constraint with central value 0 and width 1. For the systematic error in experimental data, we know that it is 3% for all recoil parameters, and we assume that they are 100% correlated. The covariance matrix is already explained in section 5.4.1.

5.6 Systematic error of lattice results

The systematic error budget for h_+ and h_- is shown in Table 5.7. We discuss the sources of error in detail here. Here, we first talk about how we get these numbers for different sources of error.

5.6.1 Error in the kappa tuning correction

We estimate that the systematic error due to the kappa tuning correction is negligible. For completeness, we discuss in detail how we make this estimation. For the kappa tuning,

Table 5.7. Systematic error budget.

source	$h_+(\%)$	$h_-(\%)$
κ-tuning adjustment	≤ 0.1	≤ 0.1
Lattice scale r_1	0.2	≤ 0.1
Heavy quark discretization	2.0	10.0
Light quark and gluon discretization	≤ 0.1	≤ 0.1
Finite volume	≤ 0.1	≤ 0.1
Electromagnetic effects	0.7	0.7
Isospin effects	≤ 0.1	≤ 0.1
Light quark mass tuning	≤ 0.1	≤ 0.1
ρ factor	0.4	20.

if we consider formula $\delta f = df/dm_2^{-1}\delta m_2^{-1}$, we see that the systematic error comes from two parts. One part is due to the uncertainty in our fit result for the slope df/dm_2^{-1}, and another part is due to the uncertainty in the kappa tuning itself.

For h_+, the total error due to the kappa tuning uncertainty is smaller than 0.08% (mainly from the uncertainty of slope). To obtain this number, we use the fact that the error is proportional to $w-1$, and we consider the worst case of momentum $(2,0,0)$. We use same assumption for h_-.

For h_-, the main source of the systematic error in the kappa tuning adjustment is from the determination of the slope. The error, including the slope error, is about 1.4%.

We determined that for f_+, we will also get a systematic error for 0.02% from h_-, and will get 0.07% from h_+. These estimates use the fact that our data are all within range $w < 1.2$. So at $w = 1.2$, the net systematic error from the kappa tuning correction is about 0.1%, much smaller than the statistical error of 1%. The same consideration applies for f_0: the systematic error from the kappa tuning correction is negligible.

5.6.2 r_1 scaling error

Our results depend, to some extent, on knowing the lattice spacing a (or scale) in physical units. Uncertainties in the determination of the spacing lead to systematic errors. Our collaboration determines the scale in two steps. (1) We choose a quantity that can be precisely measured in lattice units. For this thesis, we use the parameter r_1. It is derived from the potential $V(r)$ between two infinite-mass quarks separated by distance r. Parameter r_1 is defined implicitly by the equation $r_1^2 F(r_1) = C$ where $F(r) \equiv dV/dr$ and $C = 1$. We determine r_1/a for each ensemble (2) The parameter r_1 is not measured in experiment, so to determine its value, we measure an experimentally measurable quantity,

in this case the pion decay constant af_π in lattice units. Since f_π can be determined by experiment, and we know r_1/a from lattice calculation, we can then determine lattice spacing and r_1 unit. The value we use is 3.117(22). This lattice scale appears in only a few places in our analysis—namely in the tuning of kappa and in the calculation of the chiral log term. To determine the error due to the setting of the lattice scale, we test how much our results shift when we change r_1 by one standard deviation, namely $r_1 = 0.3139$. We find that the change in the form factor is smaller than 0.2%.

5.6.3 Light quark and gluon discretization error

In the scheme of power counting, we have the light quark and gluon discretization error of order $\mathcal{O}(\alpha_s a^2)$ and $\mathcal{O}(\alpha_s^2 a^2)$ [8]. So this source of error is already absorbed into the statistical error of coefficient of a^2 term in Equation (5.31). So the error due to light quark and gluon discretization error is smaller than 0.1%.

5.6.4 Heavy quark discretization error

If the lattice cutoff $1/a$ is not much larger than the quark masses m_c and m_b, we expect our result will deviate from continuum values. This is called heavy quark discretization error. We expect it to be the largest systematic error. We estimate [8] that it is about 1% at zero recoil, while the largest one, for a region around $w = 1.2$, it is about 2%. For simplicity, we use a universal 2% in this estimation.

5.6.5 ρ factor

As discussed in Chapter 4, the ρ factor is used to determine the normalization factor Z^μ_{cb}. They are calculated in lattice perturbation theory to one loop order. The error comes from the neglect of higher orders. We conservatively estimate the 1-loop renormalization factor of V^4_{cb}, so-called ρ^4_{cb}, has correction due to higher order perturbation terms as large as 0.4%. However, our colleagues have not finished the calculation of ρ^1_{cb}, so we use a conservative 20% systematic error due to this lack of knowledge. This could be the largest systematic error.

5.6.6 Finite-volume corrections

The spatial lattice volumes range from 64^3 to 192^3, which could distort the results from the desired infinite volume values. It was estimated in [8] to be of order 10^{-4}.

5.6.7 Light spectator quark mass tuning

On some ensembles, the strange sea quark mass was not well tuned, as much as 30% high. We expect heavy quark processes to be quite insensitive to sea quark masses. Still, we must consider it as a possible source of error. We use the same method as in section 5.6.8.

5.6.8 Electromagnetic effects and isospin correction

In our calculation, we have assumed the up and down masses are the same. In nature, they are not, of course. So if we distinguish between them in calculating the value of the form factors at the physical point, we get a slightly different result. To determine the variation of f_+ and f_0, we evaluate our fit function at m_u and m_d, instead of $m_l = (m_u + m_d)/2$. We get a shift in the form factor of 0.05% approximately. So this is a very small contribution to our systematic error, and we can ignore it.

The EM effect is also small. We comment on it briefly. We assume that half of the decays are neutral (B^0) and half are charged [33] (B^+). One correction, the Sirlin factor [34], requires dividing the experimental data by 1.0062. This is corresponding to all events detected by experiment. Then in the neutral decays, we need to divide the form factor by $1 + \alpha\pi/4$ [33], which is 1.0057, to correct for photon exchange in the final state. But this is only corresponding to half of the event detected. As we see, this is altogether a correction of 0.7%, so it is a very small correction since we assume a 3% systematic error from experiment. We can ignore this error.

5.6.9 z expansion truncation error

We have truncated the z expansion. This introduces a possible systematic error. We do this by comparing results obtained by going up to quadratic and cubic order. When the result stablized and did not change as we add higher terms with suitable priors, the statistical errors then include the truncation error. So we do not count this error separately.

5.7 Results

In Figure 5.4, we show the independent fit of f_+ and f_0. We see that the fit curve goes through the data point, and the kinematic constraint at $q^2 = 0$ is automatically met without first imposing it. For the fit without lattice systematic error, f_+ is 0.685 at kinematic point, while f_0 is 0.692 at kinematic point. So the difference is 0.007, while the error of them at this point is about 0.05. For the fit with lattice systematic error, f_+ is 0.702 at kinematic point, and f_0 is 0.712, so the difference of them is about 0.01, while the error of them is about 0.05 again. The result of fits with both systematic error and statistic error are shown

in Figure 5.5. We see from Table 5.8 that the fit result does not change when we add higher order of z. Here, for the fit of z^2 order, I do not add any prior. However, for the fit of cubic term or 4th term, I add prior with central value as zero and width as one.

We collect lattice data and experimental data, both of which contain statistical error and systematic error. And we do z expansion fit, whose result is in Table 5.9. We also get the plot of this fit in Figure 5.6. For this test, we do the fit up to z^2 and z^3. We decided to use the one with the cubic term as our final result. In this fit, we get $|V_{cb}|$ as 0.0399(19). After we get the blinding factor, we have corrected value of $|V_{cb}|$ as 0.0402(20).

5.8 Result and outlook

We conclude that the result from $B \to Dl\nu$ at nonzero recoil is $|V_{cb}| = 0.0402(20)$. This result is consistent with the recent Gambino-Schwanda inclusive (nonlattice) determination [7], which is $0.0424(9)_{exp-thy}$ within 1σ. Another project in our collaboration has exclusive $B \to D^* l\nu$ determination of $|V_{cb}|$. That project has a result of $0.0390(5)_{exp}(5)_{lat}(2)_{QED}$ [35]. This result is obtained at zero recoil, and deviates from the Gambino-Schwards result by 3σ. These results are shown in Figure 5.7.

Our large error, compared with $B \to D^* l\nu$, is mainly from the heavy quark discretization error and the matching factor ρ_1. As we mentioned in the error budget, based on power counting, the discretization error of h_+ is of order $\mathcal{O}(\alpha_s(\Lambda/2m_Q)^2)$, while h_- is of order $\mathcal{O}(\alpha_s\Lambda/2m_Q)$, so one will see that the main contribution of heavy quark discretization error is from h_-. If we use $\alpha_s = 0.3$, $\Lambda = 500$ MeV, and $m_c = 1.2$ GeV, one can check that h_+ has a discretization error of about 2%, while h_- has discretization error of about 10%. For the zero recoil determination of $B \to D^* l\nu$ determination, we do not have error from h_-. Thus, the error is smaller. As to the matching factor ρ_1, the uncertainty is large since we have not finished doing this calcaulation, and we make the assumption that it is close to ρ_4. So once we finish the perturbation calculation of ρ_1, we can reduce the systematic error from lattice input.

Compared with the error from the lattice input, the error from experiment is the main error source of $|V_{cb}|$. We do not have full information about the systematic error in the experimental data points over the full w range. We have assumed provisionally that they are fully correlated and take the value 3% at the full kinematic range. Once this information is provided, we can update our error in $|V_{cb}|$. In conclusion, the tension beween the inclusive and exclusive determinations still exists; indeed, it has worsened. However, with the new exclusive $|V_{cb}|$ values, the unitarity property of CKM matrix is good, so we found no sign for a break down of the standard model.

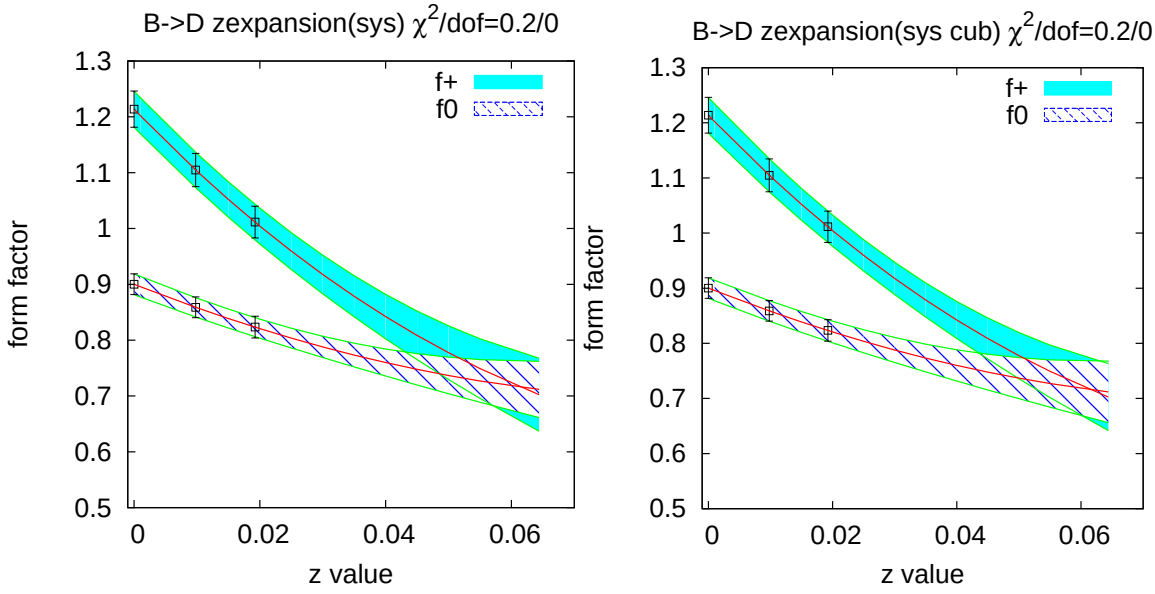

Figure 5.4. Result of the z expansion fit of the lattice values. The expansion is truncated after the quadratic term (left) and the cubic term (right). The kinematic constraint $f_+ = f_0$ is not imposed at $q^2 = 0 (z = 1.58)$. We see that even so, it is satisfied to a good approximation.

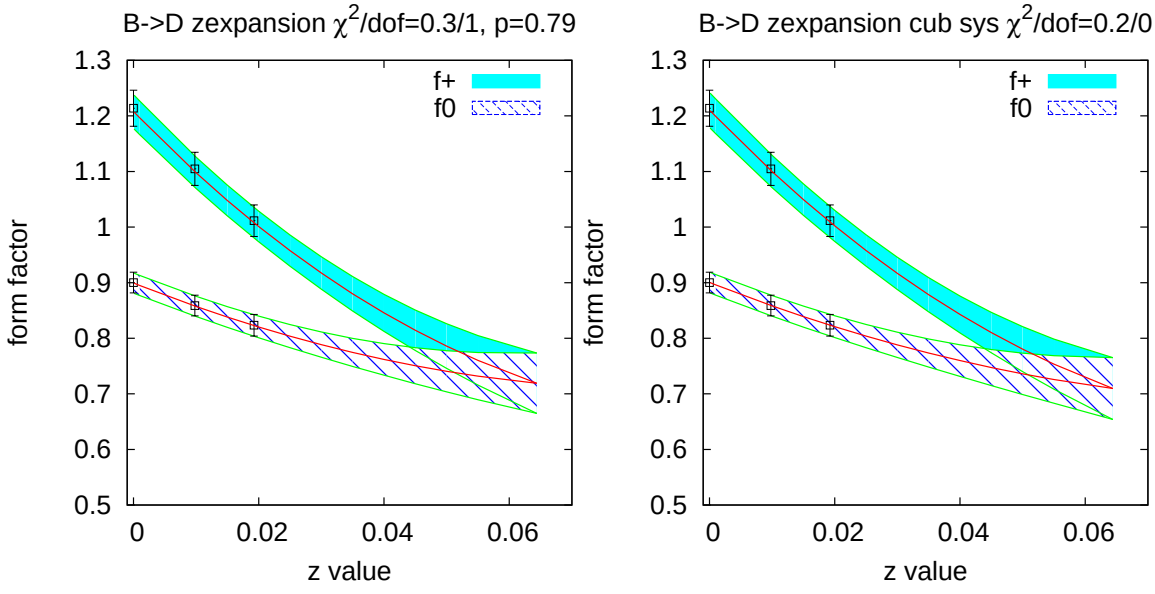

Figure 5.5. Result of the z expansion fit of the lattice values. The expansion is truncated after the quadratic term (left) and cubic term (right). The fit includes the kinematic constrain. The blue band is the error band of f_+, while the slashed band is the error band of f_0.

Table 5.8. Best fit values of parameters from the z expansion fit to lattice values of f_+ and f_0 using different procedures.

par	quadratic	cubic	quartic	f_+only(quad)	$f_0$only(quad)	f_+only(cubic)	$f_0$only(cubic)
a_0	0.01260(32)	0.01263(33)	0.01263(33)	0.01265(34)	0.0	0.01266(34)	0.0
a_1	-0.099(6)	-0.099(6)	-0.099(6)	-0.099(6)	0.0	0.099(6)	0.0
a_2	0.53(13)	0.48(15)	0.48(15)	0.47(15)	0.0	0.47(16)	0.0
a_3	0.0	0.2(8)	0.2(8)	0.0	0.0	0.014(99)	0.0
a_4	0.0	0.0	0.020(999)	0.0	0.0	0.0	0.0
a'_0	0.01138(23)	0.01136(23)	0.01139(24)	0.0	0.01131(23)	0.0	0.01131(23)
a'_1	-0.059(5)	-0.059(5)	-0.059(5)	0.0	-0.059(5)	0.0	-0.059(5)
a'_2	0.32(14)	0.30(14)	0.30(14)	0.0	0.27(16)	0.0	0.29(15)
a'_3	0.0	-0.19(86)	-0.19(86)	0.0	0.0	0.0	0.008(999)
a'_4	0.0	0.0	-0.018(999)	0.0	0.0	0.0	0.0
$\chi^2/d.o.f.$	0.3/1	0.5/1	0.5/1	0.2/0	0.1/0	0.2/0	0.1/0

Table 5.9. Best fit values of parameters from the z expansion. Results are shown combining experimental data and lattice values for different truncations of the expansion.

par	quad	cubic	quartic
a_0	0.01256(32)	0.01262(33)	0.01262(33)
a_1	-0.100(6)	-0.100(6)	-0.100(6)
a_2	0.41(9)	0.39(11)	0.39(11)
a_3	0.0	0.12(84)	0.12(84)
a_4	0.0	0.0	0.009(999)
a'_0	0.01127(23)	0.01127(23)	0.01127(23)
a'_1	-0.060(5)	-0.060(3)	-0.060(5)
a'_2	0.19(10)	0.2(1)	0.2(1)
a'_3	0.0	-0.4(8)	-0.44(82)
a'_4	0.0	0.0	-0.04(99)
V_{cb}	0.0399(20)	0.0399(20)	0.0399(20)
$\chi^2/d.o.f.$	11.8/10	11.2/10	11.2/10

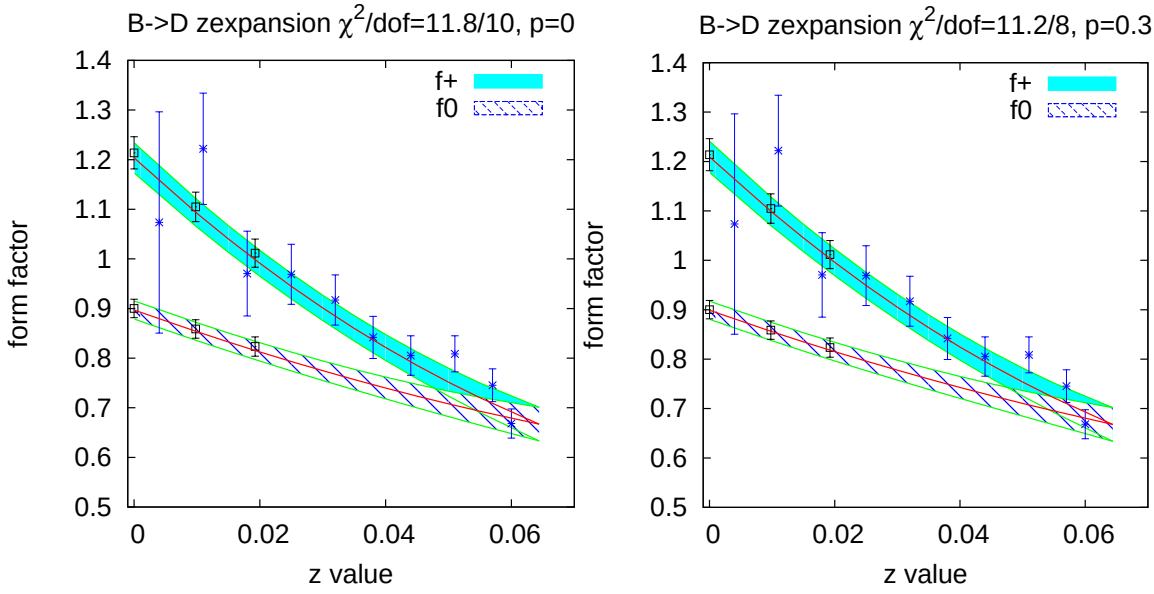

Figure 5.6. Result of the joint fit of the BaBar experimental data and lattice values up to z^2(left) and z^3(right). The black data points and error bars are for lattice synthetic data. The black data points are for the BaBar experiment. The blue band is error band of f_+, the slashed band is the error band of f_0. When adding experimental data, we have better control of the error near kinematic point $q^2 = 0$. So we see smaller error at kinematic point comparing to Figure 5.5.

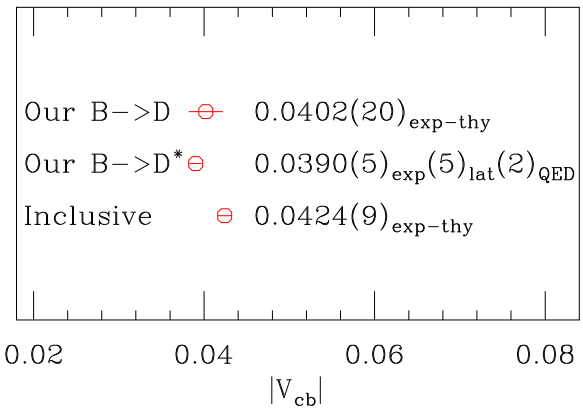

Figure 5.7. Comparison between exclusive determination and inclusive determination of $|V_{cb}|$.

APPENDIX

CHIRAL LOGARITHM FORMULA

Here is the formula we need to calculate the lattice logarithm term induced by the one loop correction of $B \to Dl\nu$ process.

$$\begin{aligned} F^+(w,m,x) &= -2[(w+2)I_1(w,m,x) + (w^2-1)I_2(w,m,x) \\ &\quad -\frac{3}{2}I_3(w,m,x) - \frac{3}{2}I_3(w,m,0)] \end{aligned} \tag{A.1}$$

with $I_i(w,m,x) = -\left[m^2 x E_{1,2}(w) + m^2x^2 \ln\left(\frac{m^2}{\Lambda^2}\right) G_i(w) + m^2x^2 F_i(w,x)\right]$
Here, $x = \Delta^{(c)}/M_j$ where M_j is the corresponding meson mass. The $D - D^*$ splitting is $\Delta^{(c)} = 140.6$MeV.

where we have:

$$\begin{aligned} E_1(w) &= \frac{\pi}{w+1} \\ E_2(w) &= \frac{-\pi}{(w+1)^2} \\ E_3(w) &= \pi \\ G_1(w) &= \frac{-1}{2(w^2-1)}[w - r(w)] \\ G_2(w) &= \frac{1}{2(w^2-1)^2}[w^2 + 2 - 3wr(w)] \\ G_3(w) &= -1 \end{aligned} \tag{A.2}$$

with $r(w) = \frac{1}{\sqrt{w^2-1}} \ln(w + \sqrt{w^2-1})$.

$$\begin{aligned} F_1(x,w) &= \frac{1}{x^2}\int_0^{\pi/2} d\theta \frac{a}{1 + w\sin 2\theta} \\ &\quad \left\{\pi\left(\sqrt{1-a^2} - 1\right) - 2\left[\frac{1}{2}\sqrt{a^2-1}\ln\left(1 - 2a(a + \sqrt{a^2-1})\right) - a\right]\right\} \\ F_2(x,w) &= \frac{1}{x^2}\int_0^{\pi/2} d\theta \frac{a\sin 2\theta}{(1 + w\sin 2\theta)^2}\left\{\frac{-3\pi}{2}\left(\sqrt{1-a^2} - 1\right) + \frac{\pi a^2}{2\sqrt{1-a^2}}\right. \\ &\quad \left. + \left[\left(\frac{3 - 4a^2}{\sqrt{a^2-1}}\right)\left(-\frac{1}{2}\ln(1 - 2a(a + \sqrt{a^2-1}))\right) - 3a\right]\right\} \\ F_3(x,w) &= \frac{1}{x}\left\{\pi\left(\sqrt{1-x^2} - 1\right) - 2\left[\frac{1}{2}\sqrt{x^2-1}\ln(1 - 2x(x + \sqrt{x^2-1})) - x\right]\right\} \end{aligned} \tag{A.3}$$

where $a = (x \cos\theta)/(\sqrt{1 + w \sin 2\theta})$.

REFERENCES

[1] E. Lunghi and R. S. V. D. Water. private communication.

[2] T. Ohl and T. H. Darmstadt, "feynmf: Drawing feynman diagrams with latex and metafont," 1995.

[3] C. Bernard, "private communication." 2013.

[4] J. H. Christenson, J. W. Cronin, V. L. Fitch, and R. Turlay, "Evidence for the 2π decay of the k_2^0 meson," *Phys. Rev. Lett.*, vol. 13, pp. 138–140, Jul 1964.

[5] J. Laiho, E. Lunghi, and R. S. V. de Water, "Lattice QCD inputs to the CKM unitarity triangle analysis," *Phys. Rev.*, vol. D81, p. 034503, 2010.

[6] S. Hashimoto, A. S. Kronfeld, P. B. Mackenzie, S. M. Ryan, and J. N. Simone, "Lattice calculation of the zero recoil form factor of $\overline{B} \to D^* l\overline{\nu}$: Toward a model independent determination of $|V_{cb}|$," *Phys. Rev.*, vol. D66, p. 014503, 2002.

[7] P. Gambino and C. Schwanda, "Inclusive semileptonic fits, heavy quark masses, and $|V_{cb}|$," 2013.

[8] J. Laiho, "private communication." proceeding of $B \to D^* l\nu$ zero recoil lattice calculation, 2013.

[9] B. R. John F.Donoghue, Eugene Golowich, *Dynamics of the standard model*. Cambridge University Press, 2002.

[10] Wikipedia, "Standard model of elementary particles." 2013.

[11] G. Zweig, "An SU(3) model for strong interaction symmetry and its breaking. 2.," 1964.

[12] D. J. Gross and F. Wilczek, "Asymptotically free gauge theories. i," *Phys. Rev. D*, vol. 8, pp. 3633–3652, Nov 1973.

[13] S. Weinberg, "A model of leptons," *Phys. Rev. Lett.*, vol. 19, pp. 1264–1266, Nov 1967.

[14] R. P. Feynman, "The theory of positrons," *Phys. Rev.*, vol. 76, pp. 749–759, Sep 1949.

[15] J. F. Donoghue, E. Golowich, and B. R. Holstein, "Dynamics of the standard model," *Camb. Monogr. Part. Phys. Nucl. Phys. Cosmol.*, vol. 2, pp. 1–540, 1992.

[16] N. Cabibbo, "Unitary symmetry and leptonic decays," *Phys. Rev. Lett.*, vol. 10, pp. 531–533, Jun 1963.

[17] J. Beringer *et al.*, "Review of particle physics," *Phys. Rev. D*, vol. 86, p. 010001, Jul 2012.

[18] M. Golterman, "Applications of chiral perturbation theory to lattice QCD," pp. 423–515, 2009.

[19] A. V. Manohar and M. B. Wise, *Heavy quark physics*. Cambridge University Press, 2000.

[20] C.-K. Chow and M. B. Wise, "Corrections from low momentum physics to heavy quark symmetry relations for $B \to \mathrm{De}\overline{\nu}_e$ and $B \to D^* e\overline{\nu}_e$ decay," *Phys. Rev. D*, vol. 48, pp. 5202–5207, Dec. 1993.

[21] J. A. Bailey *et al.*, "$B_s \to D_s/B \to D$ Semileptonic Form-Factor Ratios and Their Application to $\mathrm{BR}(B_s^0 \to \mu^+\mu^-)$," *Phys. Rev.*, vol. D85, p. 114502, 2012.

[22] M. Antonelli *et al.*, "Flavor Physics in the Quark Sector," *Phys. Rept.*, vol. 494, pp. 197–414, 2010.

[23] B. Aubert and 499 others, "Measurement and interpretation of moments in inclusive semileptonic decays $\overline{B} \to X_c \ell^- \overline{\nu}$," *Phys. Rev. D*, vol. 81, p. 032003, Feb. 2010.

[24] G. Lepage, "Lattice QCD for novices," pp. 49–90, 1998.

[25] A. Bazavov, D. Toussaint, C. Bernard, J. Laiho, C. DeTar, L. Levkova, M. B. Oktay, S. Gottlieb, U. M. Heller, J. E. Hetrick, P. B. Mackenzie, R. Sugar, and R. S. Van de Water, "Nonperturbative qcd simulations with $2 + 1$ flavors of improved staggered quarks," *Rev. Mod. Phys.*, vol. 82, pp. 1349–1417, May 2010.

[26] H. Nielsen and M. Ninomiya, "A no-go theorem for regularizing chiral fermions," *Physics Letters B*, vol. 105, pp. 219 – 223, 1981.

[27] A. X. El-Khadra, A. S. Kronfeld, and P. B. Mackenzie, "Massive fermions in lattice gauge theory," *Phys. Rev.*, vol. D55, pp. 3933–3957, 1997.

[28] M. Golterman, "QCD with rooted staggered fermions," *PoS*, vol. CONFINEMENT8, p. 014, 2008.

[29] A. Bazavov *et al.*, "B- and D-meson decay constants from three-flavor lattice QCD," *Phys. Rev.*, vol. D85, p. 114506, 2012.

[30] J. L. Richardson, "The Heavy Quark Potential and the Upsilon, J/psi Systems," *Phys. Lett.*, vol. B82, p. 272, 1979.

[31] C. Bernard, C. E. DeTar, M. D. Pierro, A. X. El-Khadra, R. T. Evans, *et al.*, "The $\bar{B} \to D^* \ell \bar{\nu}$ form factor at zero recoil from three-flavor lattice qcd: A model independent determination of $|V_{cb}|$," *Phys. Rev.*, vol. D79, p. 014506, 2009.

[32] C. G. Boyd, B. Grinstein, and R. F. Lebed, "Constraints on form-factors for exclusive semileptonic heavy to light meson decays," *Phys. Rev. Lett.*, vol. 74, pp. 4603–4606, 1995.

[33] D. Atwood and W. J. Marciano, "Radiative corrections and semileptonic B decays," *Phys. Rev.*, vol. D41, p. 1736, 1990.

[34] W. J. Marciano and A. Sirlin, "Improved calculation of electroweak radiative corrections and the value of V_{ud}," *Phys. Rev. Lett.*, vol. 96, p. 032002, Jan 2006.

[35] S.-W. Qiu, "Lattice conference talk." Semileptonic decay B→D$^{(*)}$ at nonzero recoil, 31st international symposium on lattice field theory, July 29–August 03 2013, Mainz, Germany.